Oxygen adsorption on Ag(111): A density-functional theory investigation

Wei-Xue Li,[1] Catherine Stampfl,[1,2] and Matthias Scheffler[1]

[1]*Fritz-Haber-Institut der Max-Planck-Gesellschaft, Faradayweg 4-6, D-14195 Berlin-Dahlem, Germany*
[2]*Department of Physics and Astronomy, Northwestern University, Evanston, Illinois 60208-3112*

The oxygen/silver system exhibits unique catalytic behavior for several large-scale oxidation (and partial oxidation) industrial processes. In spite of its importance, very little is known on the microscopic level concerning the atomic geometry and chemical nature of the various O species that form. Using density-functional theory within the generalized gradient approximation, the interaction between atomic oxygen and the Ag(111) surface is investigated. We consider, for a wide range of coverages, on-surface adsorption as well as surface-substitutional adsorption. The on-surface fcc-hollow site is energetically preferred for the whole coverage range considered. A significant repulsive interaction between adatoms is identified, and on-surface adsorption becomes energetically unstable for coverages greater than about 0.5 monolayer (ML) with respect to gas-phase O_2. The notable repulsion even at these lower coverages causes O to adsorb in subsurface sites for coverages greater than about 0.25 ML. The O-Ag interaction results in the formation of bonding and antibonding states between Ag $4d$ and O $2p$ orbitals where the antibonding states are largely *occupied*, explaining the found relatively weak adsorption energy. Surface-substitutional adsorption initially exhibits a repulsive interaction between O atoms, but for higher coverages switches to *attractive*, towards a $(\sqrt{3} \times \sqrt{3})R30°$ structure. Scanning tunneling microscopy simulations for this latter structure show good agreement with those obtained from experiment after high-temperature and high-O_2-gas-pressure treatments. We also discuss the effect of strain and the found marked dependence of the adsorption energy on it, which is different for different kinds of sites.

I. INTRODUCTION

Silver is a uniquely effective catalyst for ethylene epoxidation and partial oxidation of methanol to formaldehyde; the technological importance of these reactions has stimulated huge efforts in an attempt to understand the interaction of oxygen with silver, which is generally accepted to play a crucial role in its catalytic activity.[1] Nevertheless, there are still many fundamental issues that are unclear and in debate: for example, the role of atomic and molecular oxygen in the reaction of ethylene epoxidation and the various atomic oxygen species in the partial oxidation of methanol, i.e., *on-surface, subsurface and bulk-dissolved*.[2–7] Part of the reason for this lack of understanding is that these reactions and the formation of the different oxygen species take place under high-temperature and -pressure conditions. Furthermore, the relative stability of the various oxygen species depends on the experimental conditions and they can be present simultaneously depending on the temperature and pressure.[8] Thus, characterization on an atomic level is more difficult compared to the well-controlled conditions of the surface science approach of ultrahigh-vacuum (UHV) conditions and the well-developed surface characterization techniques. In the present paper we focus on the interaction of atomic oxygen with the (111) surface and begin with a brief review of reported structures and behavior.

Experimental studies on the O/Ag(111) system are somewhat difficult due to the low sticking coefficient of about 10^{-7} for dissociative adsorption of oxygen, as compared to 10^{-4} for the case of Ag(110), thus requiring high-pressure dosing in UHV (Refs. 9–12) or the use of a highly oxidative molecule such as NO_2.[13] Rovida *et al.*[9] were the first to iden-

tify a $p(4 \times 4)$ oxygen structure on Ag(111) by low-energy electron diffraction (LEED), which forms for pressures in the range from about 0.1 up to 100 Pa and at room temperatures up to ≈ 500 K. It was speculated that the structure corresponded to an $Ag_2O(111)$ plane, involving a layer of oxygen atoms between two planes of silver atoms. More detailed investigations were subsequently performed by Campbell,[10,11] who found with dosing of O_2 at 490 K that atomic oxygen exists in islands with local coverage $\Theta = 0.41$ which displayed a similar $p(4 \times 4)$ LEED pattern. It was proposed that the structure consisted of an Ag layer surrounded by two oxygen layers. Bare *et al.*[13] obtained the $p(4 \times 4)$ structure in UHV using moderate dosing pressures of NO_2; here the absolute coverage of oxygen was estimated to be 0.51 monolayer (ML). In this case a trilayer structure was proposed, like that of Campbell, but with an additional 0.14 ML of oxygen below it. Recent, high-resolution scanning tunneling microscopy (STM) images of the $p(4 \times 4)$ structure[14] show that the oxidelike layer is in registry with the underlying Ag(111) lattice.[14,15] The favored structure in this work is similar to the one proposed by Campbell, but with one silver atom in the center of the hexagonal silver ring removed. To date, the detailed atomic geometry of the $p(4 \times 4)$ structure still has not been determined unambiguously. Also, from STM studies[15] at a coverage of 0.05 ± 0.02 ML of oxygen, created after a 60-L (1 L $= 10^{-6}$ Torr sec) dose of NO_2 at 470 K, it was proposed that O is located *under* the first Ag(111) layer. Adsorption of molecular oxygen has also been observed on the Ag(111) surface, which is reported to desorb at ≈ 215 K.[10]

At *atmospheric* pressures and at *high* temperatures (around 800–900 K),[7,8,16–21] i.e., under technical methanol-

selective oxidation conditions, it has been proposed that the interaction between silver and oxygen leads to the formation of three species of atomic oxygen: namely, on-surface oxygen (O_α), "surface-embedded" oxygen (O_γ), and bulk-dissolved oxygen (O_β). Formation of O_γ is an activated process and accompanied by a significant restructuring of the surface, which consists of islands with a (111) orientation, *irrespective* of the initial crystal orientation. In particular, as characterized by reflection electron microscopy (REM), reflection high-energy electron diffraction (RHEED), and STM studies,[19] this surface exhibits a superstructure given in matrix notation as $(26 \times 1, -1 \times 26)$, and gives rise to a moiré pattern. A lateral expansion of 3% in both the [110] and [112] directions, as well as a rotation of the lattice vectors by about $2°$, was identified. Furthermore, the diffraction pattern showed third-order spots reflecting a $(\sqrt{3} \times \sqrt{3})R30°$ unit mesh (hereafter denoted as $\sqrt{3}$). The $\sqrt{3}$ periodicity was further confirmed by subsequent STM and x-ray diffraction (XRD) studies, where it was proposed that the O_γ species in this phase occupies a surface-substitutional site.[20] O_γ is reported to desorb at high temperatures ($T \approx 900$ K) and to "interact most strongly" with the silver atoms, but is *not*, however, thought to be oxidized to the binary oxide Ag_2O,[8] which is reported to be *unstable* under the formation conditions of O_γ. This oxygen species is argued to be responsible for the direct dehydrogenation of methanol.[17,22]

Various structural models have been proposed for O_γ with a $\sqrt{3}$ symmetry: It was initially suggested that O_γ is located in the subsurface octahedral site under the first Ag(111) layer;[19] this was based mainly on geometrical arguments in that the octahedral "hole" is larger than that of the subsurface tetrahedral sites. Later the same group proposed that O_γ should be on the surface due to its high reactivity to methanol in the dehydrogenation reaction.[17] On the basis of the STM studies subsequently performed, as mentioned above, a surface-substitutional site was suggested. A later study using ion scattering further supported the proposal that O_γ is surface located, but the atomic geometry proposed was a bilayer structure involving one silver and one oxygen layer.[7] A later work suggested that O_γ is located in a subsurface tetrahedral site.[21] Recently it has been reported that O_γ can be prepared by decomposing $AgNO_3$ in vacuum at 450 K (Ref. 23) [where $AgNO_3$ is formed by exposure of the Ag(111) surface to a NO/O_2 mixture at 330 K with pressures in the mbar range]. To date, the atomic geometry of the elusive, so-called O_γ species still has not been determined.

The adsorption of oxygen on silver is also of fundamental interest in relation to understanding the nature of the adsorbate-substrate bond in general and the comparison with other similar systems.[24] A number of theoretical studies have been performed for the O/Ag system; most of these studies have been performed by either cluster models[5,25–30] or have employed empirical potentials,[31–33] or have focused on the dissociation of O_2.[34–36] In the present work we report a systematic first-principles study of the coverage dependence of the physical and chemical properties of oxygen adsorption on Ag(111). We note that because the detailed atomic structure of the only two reported ordered phases of oxygen on

Ag(111) [i.e., (4×4) and $\sqrt{3}$] have not yet been identified unambiguously, a direct comparison between theory and experiment is not possible. The aim of present paper (I) and the one to follow (II) (Ref. 37) is to examine the interaction of atomic oxygen and the Ag(111) surface for various oxygen adsorption geometries using density-functional theory. In the former, we investigate on-surface and surface-substitutional adsorption, which also provides a firm basis and reference for our second paper,[37] where we investigate subsurface oxygen species and surface-oxide-like structures.

The paper is organized as follows. In Sec. II we give details of the first-principles total energy calculations, which is followed in Sec. III by our results for bulk Ag, the clean Ag(111) surface, and the O_2 molecule. The results for on-surface adsorption as a function of coverage is presented in Sec. IV, where the energetics, atomic structure, and electronic properties are analyzed. In Sec. V we discuss surface-substitutional adsorption and in Sec. VI calculated scanning tunneling microscopy images for various $\sqrt{3}$ structures are compared with experiment. The effect of strain is discussed in Sec. VII and the conclusion is given in Sec. VIII. Convergence tests are presented in the Appendix.

II. CALCULATION METHOD AND DEFINITIONS

The density-functional theory (DFT) total energy calculations are performed using the pseudopotential plane-wave method[38] within the generalized gradient approximation (GGA) for the exchange correlation functional.[39,40] The pseudopotentials are generated by the scheme of Troullier and Martins with the same functional[41,42] as used in the total energy calculations so that the treatment is consistent (see Ref. 43). The cutoff radii are $r_s = r_p = r_d = 1.4$ bohr for oxygen and $r_s = r_d = 2.42$ bohrs and $r_p = 2.62$ bohrs for silver, where for oxygen the d component acts as the local potential and for silver the s component acts as the local potential in order to remove a ghost state.[44] The wave functions are expanded in plane waves with an energy cutoff of 50 Ry and the surface is modeled by a five-layer slab separated by 15 Å of vacuum space. Oxygen is placed on one side of the slab where the induced dipole moment is taken into account by applying a dipole correction.[45] The positions of the top two (or three where stated) silver layers and adsorbate are relaxed until the forces on the atoms are less than 0.015 eV/Å. In the (1×1) surface unit cell, 21 special **k** points are used in the surface irreducible Brillouin zone (IBZ) for the Brillouin-zone integration.[46] Equivalent **k** points to these are used for all of the surface structures studied for consistency, i.e., to maximize the accuracy when comparing the energetics of different coverages as calculated in different supercells. A Fermi function is used with a temperature broadening parameter of $T^{el} = 0.1$ eV to improve the convergence, and the total energy is extrapolated to zero temperature. Convergence tests can be found in the Appendix.

We have performed calculations for oxygen in the hcp- and fcc-hollow sites for coverages ranging from 1/9 to a full monolayer. In particular, coverages of 0.11, 0.25, 0.33 and 1.0 ML were calculated using with (3×3), (2×2), $\sqrt{3}$, and (1×1) surface unit cells, respectively. Coverages $\Theta = 0.50$

and 0.75 ML were calculated in the (2×2) surface unit cell containing two and three oxygen atoms, respectively, and coverage $\Theta=0.66$ ML was calculated in the $\sqrt{3}$ unit cell containing two oxygen atoms. As noted above, equivalent special **k** points are used for all systems; this leads to 3, 6, 9, 15, 9, 6, and 21 points in the surface IBZ for $\Theta=0.11$, 0.25, 0.33, 0.50, 0.66, 0.75, and 1.0 ML, respectively. For the $\Theta=0.50$ ML structure, which has a (2×1) arrangement of O atoms in the (2×2) surface cell, the number of **k** points increases due to the lower symmetry. For substitutional adsorption with (3×3), (2×2), and $\sqrt{3}$ periodicities, the above special **k** points can be used when the oxygen sits symmetrically in the vacancy, i.e., where threefold rotational symmetry is maintained; otherwise, if the symmetry is reduced, more **k** points are required. For the (1×1) O/Ag(111) structures, we also considered bridge and top sites. These sites were found to be notably less favorable than the hollow sites; the top site is 0.93 eV less favorable than the hcp site, and when O is placed on the bridge site, it moved off this site into the fcc-hollow site. Thus, for the lower-coverage on-surface structures, we have studied only the two hollow site geometries.

It is useful to define some quantities which we evaluate in the analysis discussed below. The binding energy for oxygen adsorption per oxygen atom on the surface, $E_b^{\text{on-surf}}$, is defined as

$$E_b^{\text{on-surf}}=-\frac{1}{N_O}[E_{O/Ag}-(E_{Ag}+N_O E_O)], \qquad (1)$$

where N_O is the number of oxygen atoms in the surface unit cell, and the total energy of the adsorbate-substrate system, the clean surface, and the free oxygen atom are represented by $E_{O/Ag}$, E_{Ag}, and E_O, respectively. The binding energy is the energy that a free O atom gains by adsorbing on the surface; for on-surface adsorption it is also equal to what we call the adsorption energy, and hence $E_{ad}^{\text{on-surf}}=E_b^{\text{on-surf}}$. It is defined such that a positive number indicates that the adsorption is exothermic (stable) with respect to a free O atom and a negative number indicates endothermic (unstable). The adsorption energy per oxygen atom can alternatively be referenced to the energy which the O atom has in the O_2 molecule by subtracting half the binding energy $E_b^{O_2}$ of the O_2 molecule,

$$E_{ad(1/2O_2)}^{\text{on-surf}}=E_{ad}^{\text{on-surf}}-\frac{1}{2}E_b^{O_2}. \qquad (2)$$

Here again a positive number indicates that the dissociative adsorption of O_2 is an exothermic process, and a negative value indicates that it is endothermic and that it is energetically more favorable for oxygen to be in the gas phase as O_2.

For oxygen adsorption on the surface with a *vacancy*, the binding energy is

$$E_b^{\text{subst}}=-[E_{O/Ag}^{\text{subst}}-(E_{Ag}^{\text{vac}}+E_O)], \qquad (3)$$

where $E_{O/Ag}^{\text{subst}}$ and E_{Ag}^{vac} are the total energies of adsorbate-substrate system and the clean surface with a vacancy, re-

spectively. In this case, to obtain the *adsorption energy*, we should pay the energy cost for the formation of the vacancy, E_f^{vac},

$$E_f^{\text{vac}}=E_{Ag}^{\text{vac}}+E_{Ag}^{\text{bulk}}-E_{Ag}, \qquad (4)$$

where E_{Ag}^{bulk} is the total energy of a silver atom in bulk. This term appears since the kicked-out Ag atoms are assumed to be rebound at kink sites at steps, which contribute an energy equal to that of a bulk Ag atom (see Ref. 24). Here a positive E_f^{vac} means an endothermic process for the formation of the vacancy. The adsorption energy for substitutional adsorption, with respect to atomic oxygen, then becomes

$$E_{ad}^{\text{subst}}=E_b^{\text{subst}}-E_f^{\text{vac}}=-[E_{O/Ag}^{\text{subst}}+E_{Ag}^{\text{bulk}}-E_O-E_{Ag}]. \qquad (5)$$

Referring this energy to gas phase O_2 we arrive at

$$E_{ad(1/2O_2)}^{\text{subst}}=E_{ad}^{\text{subst}}-\frac{1}{2}E_b^{O_2}. \qquad (6)$$

To analyze the nature of bonding, it is helpful to consider the so-called *difference electron density* $n^\Delta(\mathbf{r})$,

$$n^\Delta(\mathbf{r})=n(\mathbf{r})-n^0(\mathbf{r})-n^O(\mathbf{r}), \qquad (7)$$

where $n(\mathbf{r})$ is the total valence electron density of the substrate-adsorbate system, and $n^0(\mathbf{r})$ and $n^O(\mathbf{r})$ are the electron densities of the clean substrate and the free oxygen atom, respectively, where the atomic geometry of the substrate is chosen to be that of the relaxed adsorbate system (but without the O atoms). This quantity then shows from which regions of the adsorbate/substrate system the electron density has been depleted and increased due to O adsorption on the surface. The total valence electron density is calculated as

$$n(\mathbf{r})=\int_{-\infty}^{\infty}f(\epsilon,T)n(\mathbf{r},\epsilon)d\epsilon=\sum_{i=1}^{\infty}f(\epsilon_i,T_{\text{el}})|\varphi_i(\mathbf{r})|^2, \qquad (8)$$

where $f(\epsilon,T)$ is the Fermi distribution at temperature T, and $\varphi_i(\mathbf{r})$ are the single-particle eigenfunctions of the Kohn-Sham Hamiltonian. The local density of states (DOS) is

$$n(\mathbf{r},\epsilon)=\sum_{i=1}^{\infty}|\varphi_i(\mathbf{r})|^2\delta(\epsilon-\epsilon_i), \qquad (9)$$

and the state-resolved DOS, or projected DOS, is given by

$$N_\alpha=\sum_{i=1}^{\infty}|\langle\phi_\alpha(\mathbf{r})|\varphi_i(\mathbf{r})\rangle|^2\delta(\epsilon-\epsilon_i), \qquad (10)$$

where $\phi_\alpha(\mathbf{r})$ is a properly chosen localized function. In the present work we use the eigenfunctions of the isolated pseudoatoms from which the pseudopotentials were derived for the total energy calculation.[47]

Finally, using the Helmholtz equation, we calculate the surface dipole moment (in Debye) as

$$\mu=(1/12\pi)A\,\Delta\Phi/\Theta, \qquad (11)$$

where A is the area in Å^2 per (1×1) surface unit cell, and $\Delta\Phi$ is the work-function change in eV. The work-function is calculated as the difference between the average electrostatic potential in the vacuum and the Fermi energy of the slab.

III. Ag(111) SURFACE, BULK Ag, AND THE OXYGEN MOLECULE

For bulk silver, the calculated lattice constant is $a_0 = 4.20$ Å and the bulk modulus is $\mathbf{B} = 0.87$ Mbar as obtained using the Murnaghan equation of state. The corresponding experimental data, at room temperature, are $a_0 = 4.09$ Å and $B = 1.01$ Mbar.[48] Thus, the DFT-GGA result slightly overestimates the former and, correspondingly, underestimates the latter, similar to what has been found for other metals.[43] The calculated value agrees very well with previous DFT-GGA results.[49,50] The calculated cohesive energy of fcc Ag is 2.56 eV/atom. The value reported from a full-potential linear-muffin-tin orbital (FP-LMTO) calculation using the local density approximation[51] (LDA) is 3.37 eV/atom, and the experimental result is 2.95 eV/atom.[52] The GGA result thus underestimates and the LDA overestimates the cohesive energy. Here, both calculations have been performed without the spin-polarziation correction for the free Ag atom, which is ≈ 0.18 eV.

We performed calculations for the atomic relaxation of the clean surface using (1×1), $\sqrt{3}$, (2×2), and (3×3) periodicities. These calculations provide not only a test of the surface relaxations with cell size, but are also used to evaluate the differences electron densities [cf. Eq. (7)]. We find that the interlayer distances contract only modestly in all of cases; namely, the first-second layer contraction is about 1% and the second-third layer distance is practically the same as the interlayer distance in the bulk. This is in good agreement with recent experiments using LEED which find an essentially unrelaxed surface structure [at $T = 293$ K) (Ref. 53)] and slight (0.5%) contraction at temperature 128 K (Ref. 54). The variation of the work function is negligible between our different surface cells (4.44–4.45 eV) and is in excellent agreement with experiment (4.46 eV).[55]

The total energies of isolated, free atomic oxygen and the oxygen molecule are calculated in a cubic cell of side length 15 bohrs with the **k** point (0.25, 0.25, 0.25) for the Brillouin zone sampling. The spin-polarization corrections to the O atom and the O_2 molecule are included where the values are -1.60 eV and -0.90 eV, respectively.[56] The binding energy of O_2 is calculated to be $1/2 E_b^{O_2} = 3.13$ eV per atom, the bond length $d_0 = 2.31$ bohrs, and the vibrational frequency $\omega = 174$ meV (1400 cm^{-1}). We note that the latter quantity is more sensitive to the energy cutoff, and for 75 Ry and greater, the frequency is 188 meV (1520 cm^{-1}) (see the Appendix). The experimental values are $1/2 E_b^{O_2} = 2.56$ eV, $d_0 = 2.28$ bohrs, and $\omega = 196$ meV (1580 cm^{-1}).[57] The bond length d_0 is slightly longer than the experimental value and the vibrational frequency ω slightly underestimated. The binding energy is overestimated within the GGA (which is well known) but the overbinding is notably smaller compared to the LDA result. These results are typical for well-
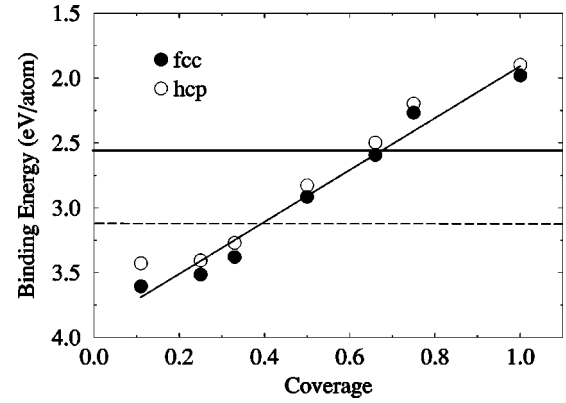
FIG. 1. Calculated binding energy of oxygen on Ag(111) in the fcc- (solid circle) and hcp- (open circle) hollow sites, for various coverages, with respect to atomic oxygen. The horizontal solid and dashed lines represent the experimental (2.56 eV) and theoretical (3.13 eV) values of the O_2 binding energy per atom. The solid line connecting the calculated binding energies is used to guide the eye.

converged DFT-GGA calculations and similar values have been obtained by, e.g., Perdew *et al.*[39] ($1/2 E_b^{O_2} = 3.12$ eV). Detailed convergence tests for the O_2 molecule are given in the Appendix. In the present work, we are interested mainly in the *relative stability* of the various structures and we consider this overbinding of O_2 when drawing any conclusions that may be affected by its explicit value.

IV. ON-SURFACE ADSORPTION

A. Energetics

The binding energies $E_b^{\text{on-surf}}$ for oxygen on the Ag(111) surface in the fcc- and hcp-hollow sites, with respect to *atomic* oxygen, are plotted in Fig. 1 and are given in Table I. It can be seen that the binding energy for O on Ag(111) decreases modestly at the beginning, from coverage 0.11 to

TABLE I. Calculated structural parameters (in Å) for various coverages Θ for O in the fcc-hollow site. R_1 indicates the bond length between oxygen and the first-nearest-neighbor silver atom, $d_{\text{O-Ag}}$ is the vertical height of oxygen above the topmost silver layer, and d_{12} and d_{23} are the first and second metal interlayer distances, where the center of mass of the layer is used. The calculated interlayer distance for bulk is 2.43 Å. $E_b^{\text{on-surf}}$ is the binding energy in eV with respect to atomic oxygen. For the 0.50 and 0.75 ML structures, there are two different O-Ag bond lengths; in the table we present the average of these.

| Coverage | R_1 | $d_{\text{O-Ag}}$ | d_{12} | d_{23} | $E_b^{\text{on-surf}}$ | |
Θ	fcc	fcc	fcc	fcc	fcc	hcp
0.11	2.18	1.24	2.42	2.42	3.61	3.43
0.25	2.17	1.22	2.41	2.42	3.52	3.41
0.33	2.18	1.28	2.41	2.40	3.38	3.27
0.50	2.15	1.22	2.41	2.44	2.92	2.83
0.66	2.15	1.22	2.40	2.41	2.59	2.50
0.75	2.16	1.27	2.41	2.43	2.27	2.20
1.00	2.17	1.34	2.40	2.41	1.98	1.90

0.25 ML, but siginifcantly and linearly with increasing coverage, which indicates that a repulsive interaction between adsorbates builds up. The fcc-hollow site is energetically favorable compared to the hcp-hollow site; however, the difference in the binding energy is small (less than 0.18 eV/atom) for the whole coverage range. Considering the binding energy of atomic oxygen on the surface with respect to half the binding energy of the (experimental) O_2 molecule, we can see that the calculations predict that coverages greater than ≈ 0.5 ML are unstable. We note that an energy barrier to dissociative adsorption could exist (and also to associative desorption) which could keep O atoms on the surface, even though the energy of O_2 in the gas phase may be lower. Actually, our calculations involving subsurface oxygen[37] show that for on-surface coverages greater than 0.25 ML, oxygen prefers to adsorb in subsurface sites and to build an oxidelike layer.

From temperature-programmed desorption (TPD) measurements, Campbell[11] estimated the binding energy of adsorbed oxygen to be 0.88 eV (at local coverage 0.41 ML). It was mentioned by Campbell that this value could include effects of bulk-dissolved, subsurface oxygen, or surface oxidelike species. When expressed with respect to atomic oxygen, the value is 3.44 eV. This value is close to our calculated binding energy for O in the fcc-hollow site at the same coverage which is 3.16 eV, but closer to that (average binding energy) of the structure at 0.5 ML involving on-surface and subsurface oxygen which is 3.27 eV [specifically one O in a (2×2) cell in the fcc site and one in a subsurface tetrahedral cite].[37]

Using DFT-GGA cluster calculations, Saravanan *et al.*[29,34] investigated oxygen adsorption on Ag(111) using an Ag_{10} cluster. The adsorption site preference they obtained is similar to ours; i.e., the fcc site is most favorable, followed by the hcp site. The adsorption energy and height of oxygen from the metal surface, however, is somewhat different to our result: The adsorption energy (referred to $1/2 O_2$) calculated by Saravanan *et al.* is 1.16 eV and the oxygen atom is 1.41 Å away from the surface, as obtained when the Ag atom is described by a nine-function minimum-basis set. However, keeping the same atomic geometry, the adsorption energy becomes 0.56 eV when using a double-ζ basis set,[34] indicating some numerical uncertainties. We may compare these results to ours for the low coverage of 0.11 ML (which provides the closest comparison to a cluster calculation since it has the minimum influence from neighboring adsorbates) where the respective values are 1.05 eV and 1.24 Å. The effect of O coverage on the adsorption energy, which is proved to be pronounced by our present work and can vary by 1.63 eV when the coverage increases from 0.11 to 1 ML, was not considered in Refs. 29 and 34.

We have also calculated the normal vibrational frequency of oxygen in the fcc site for coverage 0.25 ML by freezing the substrate geometry at the optimized equilibrium position of oxygen on Ag(111) and calculating the total energy for several different vertical displacements of O. This frozen-phonon approach is appropriate due to the considerable size mismatch between Ag and O. To calculate the frequency, we use the harmonic approximation

$$\omega = \frac{1}{2\pi}\sqrt{\frac{K}{M_O}}, \tag{12}$$

where M_O is the mass of the oxygen atom and K is the second derivative of the energy with respect to the height of oxygen at its equilibrium position. The resulting vibrational energy is 50 meV (i.e., 400 cm^{-1}). We will come back to this result later.

The interaction of O and Ag(111) is notably weaker than that of O and Ru(0001) (Ref. 58) and O and Rh(111) (Ref. 59), as may be expected due to the fully occupied d band of silver. The binding energies at coverage 0.25 are 5.55 eV and 5.22 eV for O/Ru(0001) and O/Rh(111), respectively, as compared to the value of 3.52 eV for O/Ag(111) (all quoted with respect to atomic oxygen). This stronger binding energy for O on Ru(0001) is directly reflected by the higher vibrational frequency of 64 meV (509 cm^{-1}) obtained at the same coverage.[60] For Ru(0001) and Rh(111), the dissociative adsorption of oxygen was found theoretically to be exothermic even at the high coverage of 1 ML, which was subsequently confirmed experimentally.[61,62] For O/Ag(111), on the other hand, we find that for $\Theta > 0.25$ ML a mixed phase involving on-surface and subsurface oxygen is energetically favorable as will be discussed in detail in our forthcoming publication.[37] Another important difference of O/Ag(111) to O/Ru(0001) and O/Rh(111) is the dependence of the binding energy on coverage; namely, the binding energy decreases more rapidly for O/Ag, which indicates a stronger repulsion between adatoms. As we describe below, this is due to a notably larger surface dipole moment for O on Ag(111) and a more ioniclike bonding, as compared to a more covalentlike bonding for O on Ru(0001) and O on Rh(111). It is interesting to note that for adsorption of O *under* the surface (subsurface adsorption), this trend reverses and the adsorption is more favorable at Ag(111) compared to Ru(0001) (for the 0.25 ML coverage tested).[37,63] The energy difference between the fcc and hcp sites is similar for O/Ag(111) as for O/Rh(111), while for O/Ru(0001) this difference is larger at lower coverages and only becomes small for 1 ML (see Ref.58). Also for O on Ru(0001), unlike on Ag(111), there is an *attractive* interaction between oxygen atoms in the coverage range 0.11–0.25 ML which leads to the island formation with a (2×2) structure (see, e.g., Ref. 60 and references therein).

B. Atomic structure

The relaxed atomic structure of oxygen in the fcc site on Ag(111) for the different coverages are listed in Table I. The adsorption of oxygen on Ag(111) induces only modest changes in the interlayer distances of the metal for the whole coverage range considered, for both hollow sites. In particular, there is an average contraction of the first interlayer spacing of 0.9% and 0.3 % for the fcc and hcp sites, respectively. This reflects the weak interaction between oxygen and silver. Also, the O-metal bond length does not change appreciably as a function of coverage. It varies only from 2.15 Å to 2.18 Å for the fcc-hollow site, while that for the hcp-hollow site varies in a similar manner, but the bond lengths are slightly
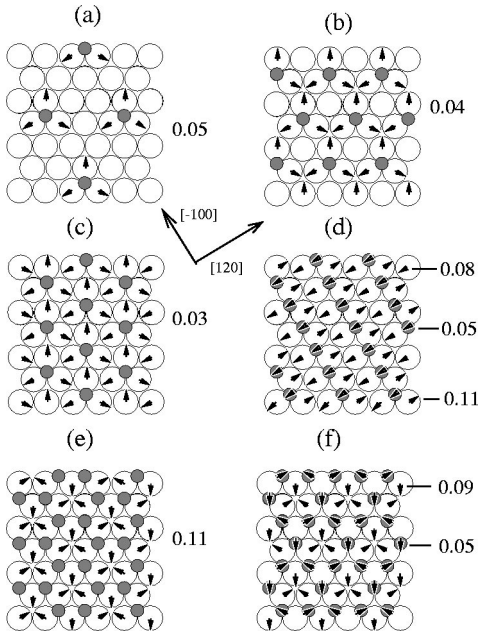
FIG. 2. Top view of the fcc-hollow O/Ag(111) systems for various coverages: 0.11 (a), 0.25 (b), 0.33 (c), 0.50 (d), 0.66 (e), and 0.75 (f) monolayers. The arrows indicate the direction of in-plane displacements, and the magnitude is given (in Å) at the right side, respectively. For the 1 ML structure (not shown) there are no in-plane displacements.

larger. The metal atoms bonded to oxygen in the top layer exhibit small lateral and vertical displacements: For O in the fcc-hollow site, at coverage 0.11, 0.25, and 0.33 ML, the three Ag atoms bonded to the O atom move radially outwards from chemisorbed oxygen by 0.05, 0.04, and 0.03 Å, respectively [see Figs. 2(a), 2(b), and 2(c)]. For coverage 0.66 ML, the lateral displacement of the three silver atoms is radially inwards towards each other, i.e., towards the vacant fcc site, by 0.11 Å [see Fig. 2(e)]. For coverage 0.50 ML, the distortion is anisotropic due to the lower symmetry. The silver atoms which bond to two oxygen atoms are displaced away from the bulk-terminated positions by 0.11 Å along the [120] direction, while the silver atoms that are bonded to just one O atom move 0.08 Å in the opposite direction, i.e., along [$\bar{1}\bar{2}0$]. Oxygen also displaces along the [$\bar{1}\bar{2}0$] direction, away from its ideal fcc-hollow site center by 0.05 Å [see Fig. 2(d)]. For 0.75 ML coverage, one surface silver atom is bonded to three oxygen atoms, and due to symmetry, its position is laterally fixed. The three remaining silver atoms in the surface unit cell are bonded to two oxygen atoms and displace radially inwards towards each other, i.e., towards the vacant fcc site, by 0.09 Å. The three O atoms are displaced by 0.05 Å radially outwards, away from the first-mentioned fixed Ag atom [see Fig. 2(f)]. All these small displacements serve to allow the O atoms to get closer to the surface and to form stronger bonds.

For the hcp-hollow site structures, a similar trend in relaxation to the fcc site is observed, but the values of displacement are slightly smaller which is due to the slightly weaker interaction between silver and oxygen for this site. The lateral atomic displacements of Ag atoms in the *second*

layer are small (i.e., <0.02 Å) for all systems. With respect to vertical rumpling in the first Ag layer, for O in the fcc-hollow site with coverages 0.11, 0.25, and 0.50, the displacements are 0.03, 0.11, and 0.06 Å, while for the hcp site the values are 0.03, 0.09, and 0.08 Å, respectively. For the 1 ML structures and the 0.33 ML and 0.66 ML structures for O in the fcc-hollow site, no buckling is present due to the constraint of symmetry, and buckling for the 0.33 ML and 0.66 ML structures with O in the hcp-hollow site and for 0.75 ML fcc- and hcp-hollow site structures is negligible.

Even though our calculations show that a full ML coverage of O on Ag(111) is unstable and subsurface O adsorption will occur for coverages >0.25 ML, from a fundamental point of view, it is still interesting to compare the on-surface coverage-dependent behavior with that of O/Ru(0001) and O/Rh(111). As mentioned above, for the O/Ag(111) systems, the first interlayer spacing does not change much with coverage. This is different to what has been found for O/Ru(0001) (Ref. 58) and O/Rh(111) (Ref. 59) where the contraction of the topmost interlayer distance of the clean metal surface (of −2.5% and −1.8%, respectively) is removed with increasing oxygen coverage, and even becomes significantly expanded at higher coverage (by 6.1% and 8.9% relative to the relaxed clean surface for 1 ML of oxygen). This difference is attributed to the considerably weaker binding energy of O to Ag(111). For the O/Ru(0001) (Ref. 58) and O/Rh(111) (Ref. 59) systems, the respective calculated bond lengths vary from 2.10 Å to 2.04 Å and from 2.00 Å to 1.95 Å for the energetically favored hollow adsorption site [i.e., hcp for Ru(0001) and fcc for Rh(111)], when Θ increases from 0.25 to 1 ML. As for O/Ag(111), it also does not significantly change with coverage, but exhibits a slight and systematic decrease with increasing coverage. For O/Ru(0001) (Ref. 58) very similar trends in structural relaxations to O/Ag(111) have been found for all coverages, which agree very well with experimental determinations by LEED analyses. For O/Rh(111) the same trend is also found at coverage 0.25 ML; however, for coverage 0.50, it exhibits the difference that the displacement of the metal atom, which is onefold coordinated to O, is in the opposite direction [see Fig. 2(d)].

It is interesting to note that on comparison of the difference charge densities for the various O/Ag(111) adlayer systems (see Fig. 4 as discussed below) with the corresponding results for O/Ru(0001) (Ref. 63) [and for O/Rh(111) (Ref. 59) at coverage 0.25 ML where comparison is possible]; it is evident that they appear exceedingly similar. In particular, the active role of the Ag d states are clearly seen, even though the top of the d band lies well below the Fermi level. The crucial difference between these systems, which gives rise to the large difference in adsorption energies, is that for O/Ru and O/Rh the antibonding O states are unoccupied, while for O/Ag, due to the filled and lower-lying metal d band, they are almost fully occupied as we will see below.

C. Electronics properties

1. Change in the work function

We turn now to analyze the electronic properties of the O/Ag(111) system, first considering the change in the work
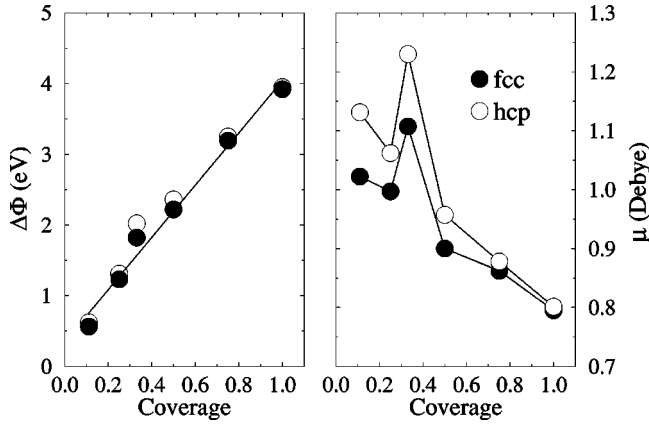
FIG. 3. Change in the calculated work function, $\Delta\Phi$ (left), and dipole moment μ (right) as a function of coverage for O in the fcc- (solid circle) and hcp- (open circle) hollow sites.

function with O coverage. The results are shown in Fig. 3. It can be seen that the work function increases linearly with coverage for both hollow sites, being slightly greater for the hcp site, and no saturation value is reached. This is due to a large (inward pointing) surface dipole moment (i.e., the negative end is outside the metal surface) arising due to a significant electron transfer from the substrate to the adatom. The large work-function increase can be expected partly due to the large difference in electronegativity between oxygen and silver of 1.54.[64] The behavior of the work-function change for O on Ru(0001) and O/Rh(111) similarly initially increases with coverage, but for a full monolayer coverage there is an indication of saturation. The electronegativity between oxygen and Ru is 1.24 and 1.16 for O/Rh(111),[64] thus notably larger for O/Ag. Consistent with this difference in electronegativities is the larger values of the work-function change for O/Ag, which is approximately twice as large compared to the O/Ru(0001) and O/Rh(111) systems.

From Fig. 3, we see that the change in the work function at coverage 0.33 ML deviates a little from the linear behavior, which results in a noticeable increase of the induced dipole moment, shown on the right side of Fig. 3. We verified that this is indeed a real effect and not, e.g., a consequence of a flat potential energy surface which we investigated by calculating the total energy of O as a function of distance from the surface. From these calculations we could also determine the perpendicular vibrational frequency which is 47 meV or 376 cm^{-1}. This is somewhat smaller than that for coverage 0.25 ML which, as mentioned above, is 50 meV or 400 cm^{-1}. The origin of the increase in the surface dipole moment for coverage 0.33 ML can be explained as follows: With the understanding that the dipole moment can be viewed as being proportional to the product of the effective charge on the O atom and the vertical distance between O and Ag, we initially consider the former. As a measure of the charge at the O atom, we calculate the dynamic charge (i.e., the slope of the curve obtained when plotting the surface dipole moment versus vertical distance of O to the surface).[24] At coverage 0.25 ML the value is 1.51 electrons, and at coverage 0.33 ML it is very similar: namely, 1.52. For a further increase of coverage, the lateral repulsive

TABLE II. Calculated structural parameters for surface-substitutional oxygen adsorption at the Ag(111) surface with different coverages Θ and symmetries (C_{3v} and C_{2v}). R_1 and R_2 are the bond lengths between oxygen and the first and second nearest-neighbor silver atoms, respectively. E_f^{vac}, E_b^{subst}, and E_{ad}^{subst} are the vacancy formation energy, the binding energy, and adsorption energy with respect to atomic oxygen, respectively. $\Delta\Phi$ is the change in the work function with respect to the clean surface. The unit of length is Å and energy is eV.

Coverage Θ	R_1	R_2	E_f^{vac}	E_b^{subst}	E_{ad}^{subst}	$\Delta\Phi$
0.11 (C_{3v})	2.45	3.03	0.55	3.34	2.79	-0.09
0.25 (C_{3v})	2.28	3.11	0.44	2.96	2.52	-0.02
0.33 (C_{3v})	2.39	3.05	0.53	3.16	2.62	-0.15
0.33 (C_{2v})	2.22	2.61	0.53	3.36	2.82	$+0.03$

O-O interaction is strengthened, and the accumulated charge on oxygen feeds back to the substrate to try and stabilize the adsorbate-substrate system—i.e., depolarization occurs—and the dynamic charge on the oxygen atom is notably reduced, e.g., to 0.48 electrons at 1 ML coverage, and consequently the surface dipole moment decreases (see Fig. 3). Considering now the vertical O-Ag distance, from Table II it can be seen that for the 0.33 ML structure, the vertical distance between O and Ag is somewhat larger; in particular, it is the largest of all the structures, with the exception of the 1 ML. Thus, the reason for the increase in the dipole moment for coverage 0.33 can be understood because the calculated charge on the O atom is practically the same as that for the lower-coverage $\Theta=0.25$ structure, but the vertical distance between O and Ag is noticeably larger. For comparison, the dynamic charge for O on Ru(0001) at coverage 0.25 ML is 1.13 electron and at 1 ML it is 0.48 electron. Thus, for O on Ag(111) at the lower coverage, there is significantly more electron charge accumulated on the O atom as compared to on Ru, indicating a more ionic bond. The value for 1 ML is the same on Ag and Ru, indicating that a saturation value has been reached.

Reported experimental values of the work-function change for O/Ag(111) are 0.55 eV, which was obtained by dosing with NO$_2$ under moderate pressures in UHV (Ref. 13) at $T=508$ K with coverage 0.51 ± 0.04 ML where the (4 $\times$4) structure forms. For high-temperature oxygen dosing under atmospheric pressure, the increase in the work function is 0.62 eV for polycrystalline Ag (Ref. 16) and 1 eV, under similar conditions, for Ag(111) (Ref. 7). The atomic geometry of these structures is clearly likely to be different from our studied ordered O adlayers, so we cannot make a straightforward comparison between theory and experiment. It is clear, however, that only for coverages <0.25 ML are the calculated values comparable to experiment. For mixed structures involving on-surface and subsurface oxygen, we find that the work function is smaller and consistent with experimental values as will be discussed in Ref. 37.

2. Difference electron density

To gain more insight into the nature of the bonding, we analyze our results by means of difference of electron densi-
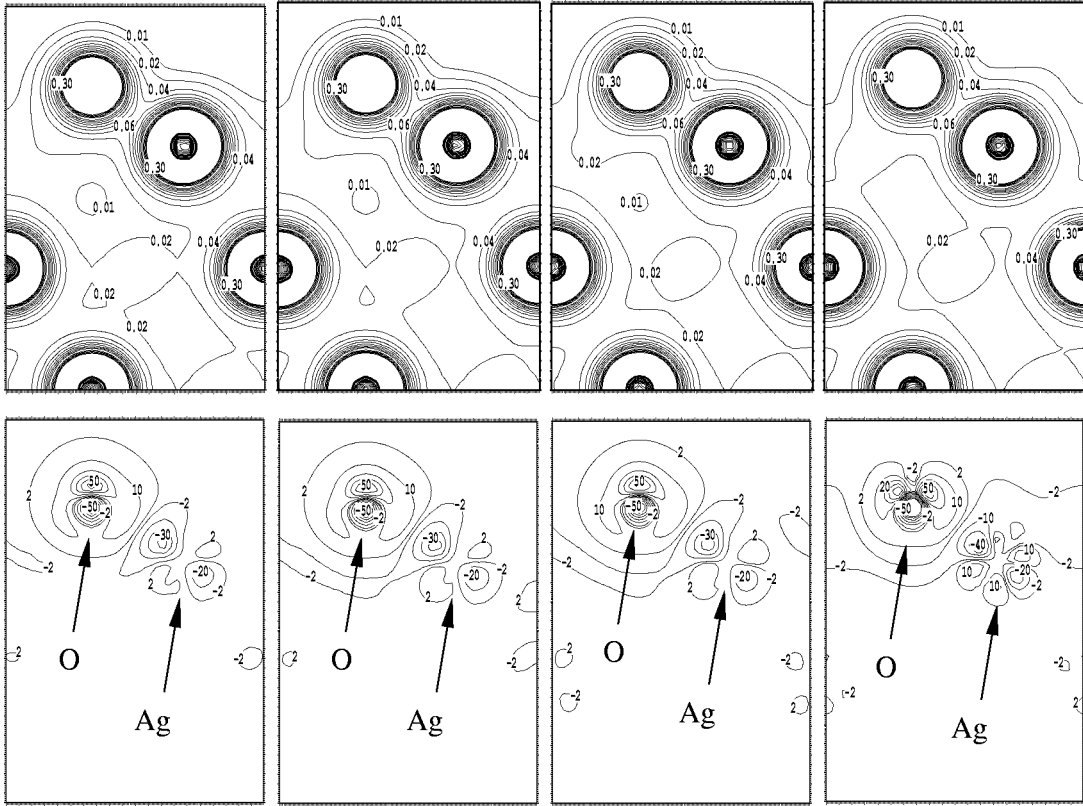
FIG. 4. Total electron density $n(\mathbf{r})$ (upper) and difference of the electron density, $\Delta n(\mathbf{r})$ (lower), for O in the fcc-hollow site for coverages 0.11, 0.25, 0.33, and 1.0 ML from left to right. The contour plane is in the [211] direction and is perpendicular to the (111) surface of the O/Ag(111) system. The unit is bohr^{-3} for $n(\mathbf{r})$ and 10^{-3} bohr^{-3} for $\Delta n(\mathbf{r})$.

ties and projected DOS (PDOS). The difference densities [defined in Eq. (7)] are shown in Fig. 4 where the corresponding total valence electron densities are also shown [cf. Eq. (8)]. Several points can be obtained: First, the perturbation of oxygen adsorption to the substrate is mainly in the topmost silver layer, which is consistent with the small difference in the binding energy between the fcc- and hcp-hollow sites. Second, the electron density around the topmost silver atom is depleted, in particular from the Ag $4d_{xz,yz}$ orbitals, while there is a significant enhancement of electron density at the O atom and also a polarization. It is immediately obvious that the shape and magnitude of the difference of electron density is very similar for coverages 0.11, 0.25, and 0.33, indicating that the bonding nature is similar. That for coverage 1.0 appears slightly different because the O atoms bond to Ag atoms that are also bonded to other O atoms. Thus, Ag-mediated lateral O-O interactions develop as indicated by the observed electron enhancement in O-$2p_{x,y}$-like states. Similar O-$2p_{xy}$ redistributions occur for the 0.50 and 0.75 ML structures (not shown) in which two or more O atoms also share an Ag atom.

3. Projected density of states

The PDOS are given in Fig. 5 for the $\Theta = 0.11$, 0.25, 0.33, and 1.0 ML structures, where the O $2p$, Ag $5s$, and Ag $4d$ orbitals are shown. The O $2s$ states (not shown) which are located from -17.15 to -16.94 eV (for lower to higher cov-

erage), with respect to the Fermi energy, exhibit a slight hybridization with the Ag $4d$ and $5sp$ orbitals. No peak is observed between the O $2s$ orbital and the lower edge of the Ag $4d$ states. We point this out because such a feature has
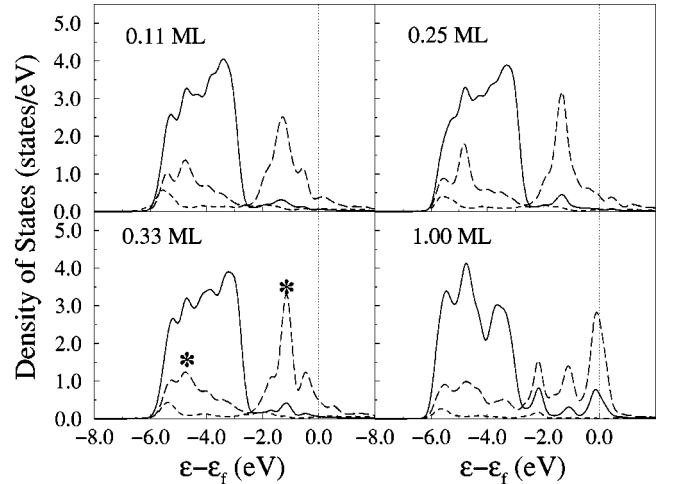
FIG. 5. Projected density of states for the O/Ag(111) system with O in the fcc-hollow sites for coverages $\Theta = 0.11$, 0.25, 0.33, and 1.0 ML. The Ag $5s$ orbital is indicated by a dashed line, the Ag $4d$ orbital by a solid line, and the O $2p$ orbital by a long-dashed line. The Fermi energy is indicated by the vertical dotted line. Stars in the $\Theta = 0.33$ ML panel indicate the states that are shown in Fig. 6.
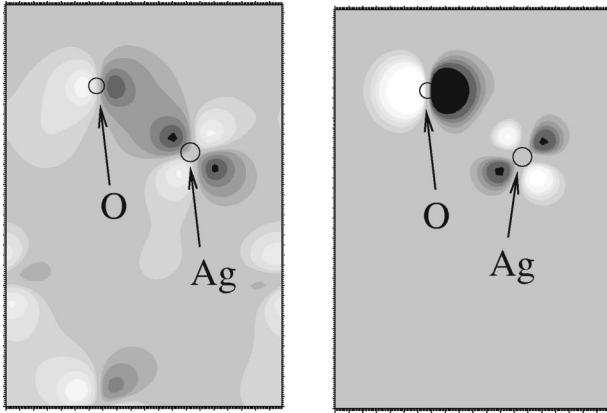
FIG. 6. Representative contour plot of the wave function of $(\sqrt{3} \times \sqrt{3})R30°$ O/Ag(111) with O in the fcc-hollow site for a bonding state (left) at energy -4.78 eV and an antibonding state (right) at energy -1.14 eV, with respect to Fermi energy at a **k** point close to the $\bar{\Gamma}$ point. The light and dark regions correspond to positive and negative components of the real part of the wave function, respectively. The smaller and large circles represent the position of the oxygen and silver atoms, respectively.

been found in some experimental studies, the origin of which is under debate (see, e.g., Ref. 6). Clearly, purely on-surface adsorbed oxygen is not responsible for these features. From Fig. 5 it can be seen that there is a hybridization between O $2p$ and Ag $4d$ orbitals for the whole coverage range considered. By examining the components of these orbitals it is found that the mixing is mainly between O $2p_{x,y}$ and Ag $4d_{xz,yz}$ components and O $2p_z$ and Ag $4d_{xz,yz}$ components for coverage 0.11, 0.25, and 0.33 ML. For coverage 1 ML, due to the strong Ag mediation, mixing between the O-$2p_{x,y}$–Ag-$4d_{xz,yz}$ and the O-$2p_z$–Ag-$4d_{xz,yz}$ states occurs, and this hybridization creates additional features, as seen in Fig. 5. This has been verified by inspection of the spatial distribution of the state wave functions. Also it can be noticed from Fig. 5 that the Ag $5s$ states hybridize with Ag $4d$ and O $2p$ states.

Considering the PDOS for the O atom, it can be seen that there are two main regions of high electron density below the Fermi level. These correspond to bonding and antibonding states, which we verified by inspection of the spatial distribution of the state wave functions. An example of such bonding and antibonding states is shown in Fig. 6 for the $\sqrt{3}$ O/Ag(111) structure with O in the fcc-hollow site, where it can clearly be seen that the left one is a bonding state and the right one is antibonding. The respective energy levels are -4.76 eV and -1.14 eV, and the **k** point used is near the $\bar{\Gamma}$ point as selected from our nine special **k**-point set. The hybridization between O $2p_{x,y}$ and Ag $4d_{zx,zy}$ is clearly indicated. The bonding state is located at the bottom of Ag $4d$ band, and the antibonding state is largely *occupied*, thus preventing a strong covalent bonding which requires that the antibonding state be unoccupied. With increasing coverage, it can be noticed that the DOS at the Fermi energy increases and further destabilizes the system in accordance with the decrease in binding energy.
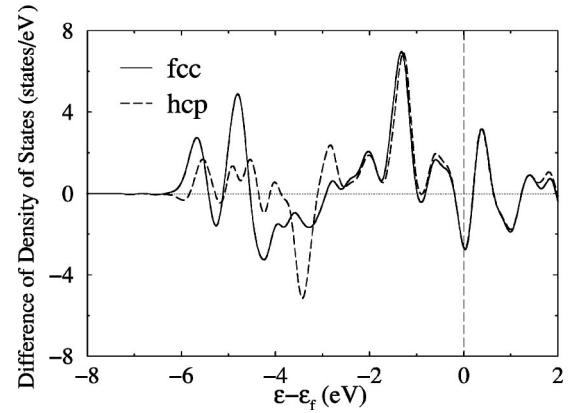
FIG. 7. Difference of the density of states for the O/Ag(111) system with O in the fcc- (solid line) and hcp- (long-dashed line) hollow sites for coverages $\Theta = 0.25$ ML. The Fermi energy is indicated by the vertical dashed line.

We now turn to compare results for O in the fcc- and hcp-hollow sites in order to try and understand the fcc preference. We do this for coverage 0.25. In Fig. 7 the difference of the density of states is shown [total DOS of the O/Ag(111) system minus those of the clean surface]. For each site bonding (at ≈ -6 to -4 eV) and antibonding states occur, where the latter are very similar for the two sites (i.e., compare the energy region from -2.5 to 2.0 eV). The bonding states, however, exhibit a difference in that for the fcc-hollow site, they lie slightly lower in energy. Other differences already noted are that the work-function change is larger for the hcp site (compare 1.31 to 1.23 eV) and the vertical O-Ag distance is slightly larger (compare 1.25 to 1.22 Å). Furthermore, the (semicore) O $2s$ level is located at -17.12 eV for the fcc-hollow site, somewhat deeper than for the hcp-hollow site where it is at -17.02 eV.

For O/Rh(111) the fcc-hollow site is also energetically favorable, and a similar correlation between the work-function change and core level shift (here the O $1s$) was observed. However in this case, just the *opposite* to O/Ag(111), the change in the work function for O in the fcc site is larger (compare 0.56 to 0.45 eV) and the O $1s$ core level of the fcc site is higher in energy (less bound, by 0.36 eV) compared to the hcp site. This was argued to indicate a stronger ionic bonding for the fcc site[59] which overcompensates the greater electrostatic repulsion and was identified as the reason for the fcc preference. Clearly this explanation does not hold for O/Ag(111). For although we indeed find that the electron charge on the hcp O of 1.65 is larger than the fcc O of 1.51, which indicates that O at the hcp site is more ionic in nature, the greater electrostatic (dipole-dipole) repulsion at the hcp site disfavors the hcp-site adsorption.

V. SURFACE SUBSTITUTIONAL ADSORPTION

Defects like vacancies, steps, and dislocations extensively exist in realistic catalysts operating under high-temperature and -pressure conditions, and can play an important role as acting as possible active sites.[15,65,66] As noted in the Introduction, the surface-substitutional site (among others) has
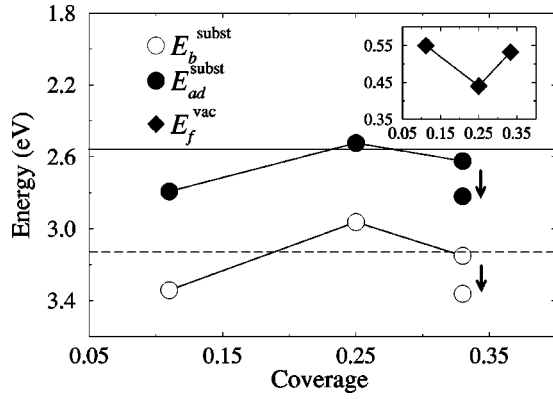
FIG. 8. The binding energy (open circles) and adsorption energy (solid circles) for surface-substitutional oxygen adsorption [for the symmetrical (C_{3v}) case] with different coverages. The formation energy of the vacancies (solid diamonds) is given in the inset as a function of coverage. The arrows indicate the energy gain obtained for the case of the reduced (C_{2v}) symmetry. The horizontal solid and dashed lines represent the experimental (2.56 eV) and theoretical (3.13 eV) values of half the binding energy of O_2, respectively.

been proposed for the experimentally observed $\sqrt{3}$ structure. In the following we therefore investigate surface-substitutional adsorption of oxygen for various coverages.

A. Vacancy formation

As a first step, we calculate the surface vacancy formation energy E_f^{vac} according to Eq. (4). The results are given in Table II and are plotted in the inset of Fig. 8. It can be seen that E_f^{vac} weakly depends on the concentration of vacancies; however, in all cases vacancy formation is endothermic which is of course expected, since otherwise the material would be unstable or just form a new surface by creation of surface vacancies. The formation energy of a vacancy is small for silver, as a noble metal; for example, for the (3 $\times$ 3) cell, i.e., concentration 0.11, we obtain $E_f^{vac} = 0.55$ eV. At a concentration of 0.25 the value is 0.44 eV which can be compared to that of 1.70 eV for a Ru vacancy at the Ru(0001) surface for the same concentration.[63] The qualitative difference in the vacancy formation energy between Ag(111) and Ru(0001) can be understood in terms of a bond-cutting model:[24] Here the energy contribution per atom, E, is assumed to be a function of its coordination C, e.g., $E(C) \propto \sqrt{C}$, where a coordination of 12 corresponds to the cohesive energy. Using this, it can be found that the surface vacancy formation energy is proportional to 0.29 times the cohesive energy,[24] where the cohesive energy is considerably smaller for Ag (compare the experimental values of 2.95 eV and 6.74 eV for Ag and Ru, respectively), yielding rough estimates for the surface vacancy formation energies of 0.86 eV and 1.95 eV. These values are overestimated within this simple model, but the trend is closely reflected.

An inward relaxation of the topmost layer is found for all surface vacancy structures considered, and increases with the vacancy concentration. The maximum inward relaxation is -4.5% for the $\sqrt{3}$ periodicity. Using the FP-LMTO method, Polatoglou *et al.*[51] calculated the formation energy of the sur-
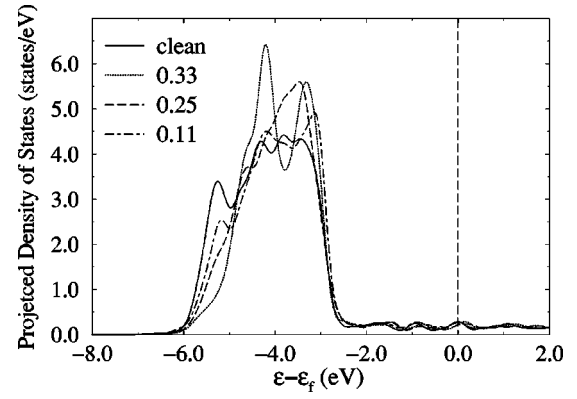
FIG. 9. PDOS for the surface silver atom at the vacancy edge with different vacancy concentrations (0.11, 0.25, 0.33). The solid line represents the clean surface and the dotted, dashed, and dot-dashed lines denote the ($\sqrt{3} \times \sqrt{3}$)$R30°$, (2×2), and (3×3) vacancy structures, respectively. The Fermi energy is indicated by the vertical dashed line.

face vacancy of Ag(111) with a $\sqrt{3}$ periodicity as 0.67 eV, which is larger than the present result of 0.53 eV. Atomic relaxation was not taken into account in the FP-LMTO calculations. However, the energy gain associated with this relaxation (comparing to a calculation with the truncated bulk geometry) is only 0.04 eV. Thus the difference from the FP-LMTO study is 0.1 eV. For a vacancy in the bulk with a $\sqrt{3}$ periodicity we obtain 0.78 eV and that obtained by the FP-LMTO method is 1.06 eV.[51] For lower-concentration bulk vacancies the values are 0.70 and 0.80 eV for (2×2) and (3×3) periodicities, respectively, thus rather similar to the $\sqrt{3}$ result. The reason for the deviation between the two calculation methods could be due to the different exchange-correlation functionals used; in the FP-LMTO work it was described by the LDA,[67] whereas in the present work we use the GGA. But other differences exist as well, as, for example, in the treatment of relativistic effects, and we also note that the FP-LMTO work was state of the art, but maybe only approximately a "full potential" for a vacancy.

The DOS of surface silver atoms at the edge of the vacancy, as well as at the perfect surface, are given in Fig. 9. Due to the decrease in coordination number from 9 (perfect surface) to 8, 7, and 6 for vacancy concentration 0.11, 0.25 and 0.33, the DOS of the surface atoms at the edge of the vacancy become sequentially narrower; i.e., this tendency is more pronounced for higher vacancy concentrations. The change is mainly due to the distortion of the Ag $4d$ band where a sequential reduction in states at the bottom of the band can be noticed. The perturbation of the atom in the second layer is smaller due to the smaller change in coordination number.

B. Energetics

We consider surface-substitutional adsorption for the (3 $\times$ 3), (2×2), and $\sqrt{3}$ structures, where the full C_{3v} symmetry of the vacancy is held; i.e., oxygen cannot displace in plane [see Fig. 10(a)]. The associated results are given in Table II, namely, the atomic structure, binding and adsorp-
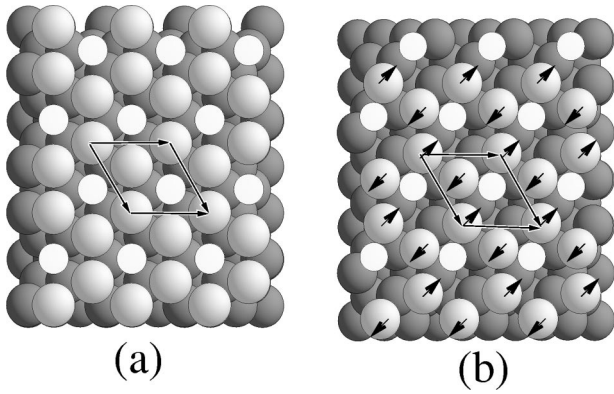
FIG. 10. The surface-substitutional structure for $(\sqrt{3} \times \sqrt{3})R30°$ O/Ag(111) with C_{3v} (a) and C_{2v} (b) symmetry. Small white circles represent the oxygen atoms; large pale and dark grey circles represent the surface and lower-lying metal atoms, respectively. The arrows in (b) indicate the direction of the in-plane displacements of (0.13 Å).

tion energies, and work-function change. The binding, E_b^{subst}, and adsorption, E_{ad}^{subst}, energies, as calculated according to Eqs. (3) and (5), are plotted in Fig. 8 with respect to atomic oxygen. It can be seen that the structure with the lowest coverage, 0.11 ML, is most favorable. A repulsive interaction between adsorbates occurs for the coverage range of 0.11–0.25, while it switches to attractive when Θ varies from 0.25 to 0.33 ML. This attractive interaction indicates island formation with a $\sqrt{3}$ structure. On comparing the energetics in Figs. 8 and 1 it can be seen that on-surface adsorption is energetically favorable compared to surface-substitutional adsorption for the coverage range of 0.11–0.33 ML. In the following we consider additional aspects of surface-substitutional adsorption.

Recently, the structure of $\sqrt{3}$ Sb/Ag(111) was determined by LEED, and the results clearly favored the surface-substitutional site, but with a stacking fault such that all outermost layer Sb and Ag atoms switched from occupying fcc sites to hcp-hollow sites.[68] Previous *ab initio* calculations had predicted that the surface-substitutional structure was energetically favorable, but did not consider the possibility of a stacking fault.[69] For $\sqrt{3}$ Sb/Cu(111) a similar result has been obtained by x-ray diffraction and medium-energy ion scattering.[70,71] We therefore studied the possibility of such a stacking fault for the $\sqrt{3}$ O/Ag(111) system. First, for the clean Ag(111) surface we find that the energy cost for creating a stacking fault in the outermost layer is only 0.002 eV per atom, i.e., *negligible*. Second, we calculated the adsorption energy for the $\sqrt{3}$ O/Ag(111) structure with the stacking fault. We find that the adsorption energy is 2.60 eV, i.e., smaller than the case without a stacking fault, but only by 0.02 eV, which is within the accuracy of our calculations.

Another consideration is that O may prefer to adsorb off center in the vacant Ag site. In order to test this, we released the symmetry constraint and displaced the oxygen away from the vacancy center but still held the mirror plane. Due to the lower symmetry, the special **k** points are increased to 21 in order to maintain equivalent sampling in the IBZ. After

optimizing the geometry, we obtain an energetically more stable structure, and oxygen approaches the edge of the vacancy. The adsorption energy increases from 2.62 eV with full C_{3v} symmetry to 2.82 eV, i.e., a *significant* energy gain of 0.20 eV. The structure is illustrated in Fig. 10(b). The oxygen atom is coordinated to four silver atoms, two in the first metal layer (the first nearest neighbors) and two in the second layer (the second nearest neighbors). We also introduced a stacking fault to this structure as before and again we did not obtain an energetically more favorable structure; the adsorption energy decreases to 2.74 eV. Oxygen could also attack the edge of the vacancy in the opposite direction, where it is coordinated to three silver atoms, two in the first silver layer, and one in the second metal layer. The obtained adsorption energy is 2.77 eV, thus energetically unfavorable compared to the (quasi-)fourfold-coordinated geometry. However, both of them are energetically more favorable than the symmetrical substitution in the vacancy center with or without a stacking fault. We also tested whether a further energy gain could be obtained by displacing the oxygen atom away from the mirror plane, i.e., by not imposing any symmetry. This was found not to be the case and no energetically more favorable structure could be obtained. Further study shows that oxygen occupation in the center of the vacancy is actually at a saddle point of the potential energy surface (PES), and O will move to the edge of the vacancy when not restricted by symmetry. The same is true at the lower coverage; however, the energy gain is smaller. The reason for the more favorable binding energy at the vacancy edge can be (qualitatively) related to the lower coordination of the Ag atoms to which the O atoms bind; these atoms have a narrower and higher-lying d-band center compared to the Ag atoms in the second layer which are even more bulk like (i.e., have a higher Ag coordination) than the Ag atoms of the unreconstructed surface and have a lower-lying d-band center. With this picture (as discussed in more detail in Sec. VI), an upshifted (or higher-lying) d-band center has been correlated with a stronger binding compared to a lower-lying one.[73] In this sense the larger energy gain for the $\sqrt{3}$ structure can be understood since the metal atoms at the edge of the vacancy in this structure have the greatest narrowing of the d band as shown in Fig. 9. Similarly, the weaker binding of the O atoms symmetrically in the vacancy, where they bond to second-layer Ag atoms, can be explained since, as mentioned above, the Ag atoms in the second layer are more bulk like, having a lower-lying and broadened d band compared to surface Ag atoms.

Even with the found energy gain due to the effect of reduced symmetry, the adsorption energy with respect to $1/2 O_2$ (experiment) is just 0.26 eV. This is still energetically unfavorable compared to on-surface adsorption at the same coverage. As mentioned above, the O_γ species with a reported $\sqrt{3}$ periodicity has only been experimentally observed after long exposure of silver at high temperature and high O_2 pressures where it has been proposed to result from segregation to the surface of a bulk-dissolved O species. With respect to the influence of temperature, we note that the relatively small formation energy of surface and bulk vacancies, together with the observation that Ag atoms become mobile at about

750 K,[72] indicates that the concentration of vacancies could be considerable at high temperature. Moreover, we find that adsorbed oxygen can give rise to a notable decrease in the surface vacancy formation energy: The energy cost to remove a non-O-bonded Ag atom from the (2×2) O structure is 0.12 eV—significantly less than the 0.44 eV for the clean surface. A similar effect has been reported for O on Ru(0001) (Ref. 63) and O on Cr(001) (Ref. 74). Oxygen adsorption at an existing vacancy (i.e., without paying the energy cost to create the vacancy, namely, the binding energy) yields a value of 3.36 eV, which is then *larger* than that for on-surface adsorption at the same coverage, which is 3.29 eV; that is, the bonding at the vacancy is stronger. Another consideration is that the configurational entropy $-k_B T \ln(N)$, where k_B is Boltzmann constant, T is the temperature, and N the number of equivalent sites, for O in the surface-substitutional site is larger than for on the surface: For the surface-substitutional site, O has three equivalent positions at the edges of the vacancy. At $T = 300$ K this contributes -0.03 eV and, at 800 K, -0.08 eV to the binding energy. If we assume that the alternative three sites at the opposite vacancy edges could be occupied with a similar probability (and they are only 0.05 eV less favorable), then this would yield six equivalent sites and a larger contribution of -0.05 eV and -0.12 eV at 300 K and 800 K, respectively. Thus, under higher-temperature conditions, it could be possible that the surface-substitutional structure forms.

C. Atomic structure

The calculated atomic structure for the surface-substitutional structures is given in Table II. The nearest-neighbor O-Ag bond length R_1, which is between O atoms and Ag atoms in the *second* metal layer, for the *symmetric* positions (threefold coordinated) are notably longer, by 0.11–0.27 Å, compared to (fcc) on-surface adsorption with the same periodicity, which indicates that the interaction between oxygen and silver is weaker in accordance with the obtained binding energies (compare Tables I and II). The second nearest-neighbor Ag atoms of oxygen (to which O is sixfold coordinated) are the silver atoms in surface layer at the edge of the vacancy. These corresponding bond lengths R_2 are given in Table II as well. With the constraint of symmetry, no corrugation occurs in the surface layer for the (2×2) and $\sqrt{3}$ structures, while a slight rumpling of 0.02 Å for the (3×3) structure occurs. Compared to the clean surface with a vacancy, the variation in the top two Ag interlayer spacings due to the presence of oxygen is very small (i.e., <0.02 Å).

For the case of reduced (C_{2v}) symmetry for the $\sqrt{3}$ structure, oxygen binds preferably to the topmost metal layer, and the nearest-neighbor metal atoms are switched from the atoms in the second layer to the atoms in the first layer, and the nearest-neighbor coordination number decreases from 3 to 2. Also the bond length between oxygen and the nearest-neighbor silver atom decreases from 2.39 Å to 2.22 Å, where the latter is close to the on-surface O-Ag bond length (2.18 Å). The second nearest-neighbor O-Ag bond length is 2.61 Å and corresponds to the Ag atoms located in the second metal
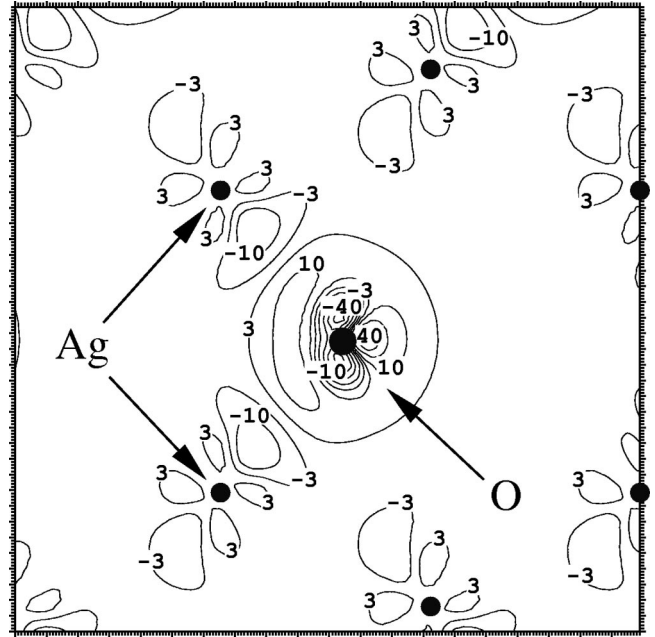
FIG. 11. Difference of electron density $n^{\Delta}(\mathbf{r})$ [cf. Eq. (7)] for the $(\sqrt{3} \times \sqrt{3})R30°$ O/Ag(111) structure for the case of surface-substitutional adsorption with the energetically favorable reduced (C_{2v}) symmetry geometry. The cross section is in the (111) plane through the oxygen atom. The large and smaller solid circles represent the positions of oxygen and silver atoms, respectively. The units are 10^{-3} bohr^{-3}.

layer. This is in line with the relation between bond length, bond strength, and coordination number as discussed in Ref. 24. That is, we have the formation of fewer but shorter (and stronger) bonds. In addition, the two Ag atoms in the top layer to which the O binds move away from each other by a large 8.4% compared to the unrelaxed value (i.e., 2.97 Å) to let oxygen get closer between them.

D. Electronic properties

The work-function change for surface-substitutional adsorption is given in Table II. It can be seen that due to the screening by surface silver atoms, there is only a minor *decrease* in the work function (except for the structure with C_{2v} symmetry where there is a minimal increase) which is very different to adsorption on the surface where it increases linearly and strongly. This small change in the work function can also be thought of as being due to the fact that O in the substitutional site sits much lower in the surface Ag layer, giving rise to a smaller perpendicular component of the induced surface dipole moment. In Fig. 11 the difference electron density for the case of reduced symmetry for the 0.33 ML structure is shown. The bonding configuration is clearly presented by the redistribution of electron density from the surface metal atoms to oxygen, and it resembles closely that for the on-surface adsorption, despite the different local atomic geometry.

For symmetric surface-substitutional adsorption, the PDOS exhibits a hybridization between O and Ag in the second layer. The PDOS of the O $2p$ orbital for the three
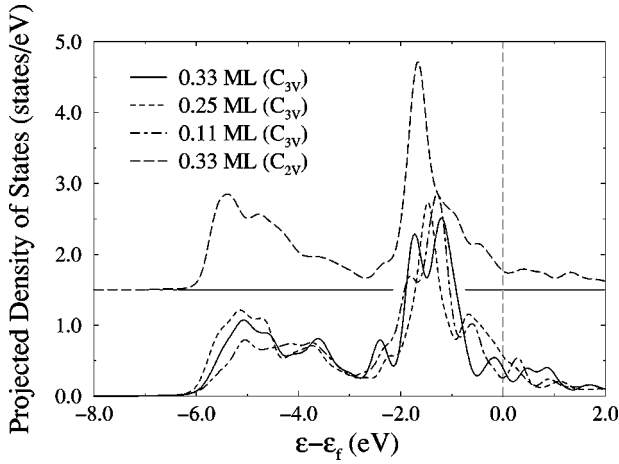
FIG. 12. Projected density of states (PDOS) for substitutional oxygen showing the O $2p$ orbital with symmetry C_{3v} for $\Theta = 0.11$ (dot-dashed line), 0.25 (dashed line), and 0.33 (solid line). The result with coverage 0.33 for reduced (C_{2v}) symmetry (long-dashed line) is also shown and is plotted with an upshift of the origin on the y axis. The Fermi energy is indicated by the vertical dashed line.

coverages are given in Fig. 12. The (2×2) structure has the highest PDOS at the Fermi energy which is in accordance with it being energetically unfavorable compared to the (3×3) and the $\sqrt{3}$ structures. We also give the PDOS of the O $2p$ orbital for the reduced (C_{2v}) symmetry with coverage 0.33 ML. It can be noticed, in comparison to the symmetric case, that there is a further slight reduction in the DOS at the Fermi level, consist with the larger binding energy found. Overall, the appearance of the PDOS of the O $2p$ orbital for the surface-substitutional structures is close to those of on-surface oxygen. From these considerations, the nature of the interaction between the surface-substitutional oxygen and the substrate is similar to on-surface adsorption. It is the screening by the surface metal atoms that gives rise to the observed difference in work-function change with coverage.

VI. SCANNING TUNNELING MICROSCOPY: COMPARISON OF EXPERIMENT AND THEORY

As mentioned above, based on our calculated adsorption energies, the surface-substitutional $\sqrt{3}$ structure is less favorable than on-surface adsorption although the binding energy is stronger. It cannot be ruled out that it may form as a consequence of high-temperature and -pressure exposure, through the formation of defect sites (i.e., Ag vacancies). STM measurements for the $\sqrt{3}$ phase have been reported[7,20]; we therefore considered it instructive to compare these results with simulations that we carry out within Tersoff-Hamann theory.[75] In this picture the tunneling current I is approximated by the local density of states (LDOS),

$$I \propto \sum_{\nu} |\varphi_{\nu}(\mathbf{r}_0)|^2 \delta\epsilon, \qquad (13)$$

where φ_{ν} is the calculated wave function of the system, $\mathbf{r}_0$ is the position of the "tip," and ν is the energy window inte-
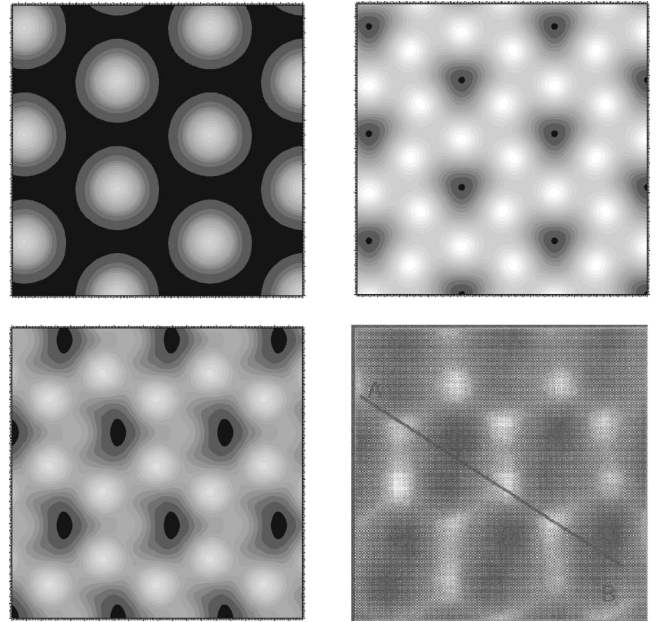
FIG. 13. Simulated STM pictures of $(\sqrt{3} \times \sqrt{3})R30°$ O/Ag(111) for O in the fcc-hollow site (top left), subsurface octahedral site (top right) and surface-substitutional site (bottom left), and experimental results (bottom right) (Ref. 20). The energy window ranges from -2 eV below the Fermi energy to the Fermi energy. The height of the "tip" is 2 Å away from the uppermost nuclei. The same area has been used in the figures.

grated. The height of the "tip" from the uppermost nuclei is taken to be 2 Å and the integrated energy window is from -2 eV below the Fermi energy to the Fermi energy. In Fig. 13 the simulated STM pictures for O in the fcc-hollow site, the subsurface octahedral site, and the surface-substitutional site with coverage 0.33 ML are given. We note that the subsurface octahedral site is that which is obtained when an on-surface fcc O atom moves directly downwards to reside between the first and second Ag layers; i.e., it bonds to three Ag atoms above it in the first layer and three below in the second layer.

In Fig. 13, for the fcc-hollow site, the bright circle corresponds to the oxygen atoms, while for the subsurface octahedral site and the surface-substitutional site, it is the surface silver atoms that appear bright. Despite the fact that it is possible that the contrast could be inverted when the interaction between the tip and the adsorbate-substrate system is included,[76] the difference between the three adsorption sites is clear enough compared to the experimental one, in that the hexagonal symmetry of the surface-substitutional site with an asymmetric "hole" agrees well with the experiments,[7,20] while the others do not.[7,20] This provides support for the existence of the $\sqrt{3}$ surface-substitutional structure. Clearly, however, this is not sufficient evidence to be able to conclude that this is the structure, and in this respect a detailed LEED intensity analysis is called for. We note that the experimental studies did not report the bias for the STM picture. We therefore tested energy windows of from -3 to 0, -1 to 0, and -0.5 to 0 eV, as well as the positive energy windows of from 0 to 0.5, 0 to 1.0, 0 to 2.0, and 0 to 3 eV. Different tip-

substrate distances varying from 1 to 4 Å from the uppermost nuclei were also checked and all results exhibited qualitatively the same results.

The vibrational frequency of so-called O_γ has been reported from surface-enhanced Raman spectroscopy (SERS) to be 100 meV (803 cm^{-1}) after Ag(111) was exposed to oxygen at elevated temperatures (~ 800 K) and atmospheric pressure[18]—that is, similar conditions to those used to create the surface investigated in the STM study—and indeed both studies (STM and Raman) assigned the O-related features to the O_γ species. Molecular oxygen was excluded due to the high temperatures used. Also, by *in situ* Raman spectroscopy, Wang *et al.*[3] studied the interaction between molecular oxygen and polycrystalline silver at atmospheric pressure and temperatures between 298 and 883 K. Raman bands at 119 meV and 99 meV (956 and 800 cm^{-1}) were observed and both of them were assigned to *atomic* species. This assignment was based on isotope labeling experiments where on replacement of $^{16}O_2$ with $^{18}O_2$ the bands shifted to 931 and 778 cm^{-1}, respectively. This shift was argued to be significantly smaller than isotopic shifts for O-O stretching vibrations of molecular oxygen species on silver; thus, the Raman bands were attributed to atomic oxygen species. However, we note that this same isotope shift of $\approx 20^{-1}$ cm for the Raman feature at 800 cm^{-1} has also been used to conclude the *molecular* origin of this oxygen,[4] thus highlighting the problem of its characterization.

For comparison we calculated the normal vibrational frequency, as well as an in-plane vibration (with mirror symmetry), for surface-substitutional adsorption with the $\sqrt{3}$ structure with the energetically favorable reduced symmetry using the harmonic approximation. The result is 26 and 37 meV (206 and 297 cm^{-1}), respectively. This is in stark contrast to the above-mentioned reported experimental values of >800 cm^{-1}. For subsurface octahedral oxygen adsorption at a coverage of 0.25 ML, we calculated the normal vibrational frequency and found it to be 46 meV (366 cm^{-1}), while the frequency for fcc-hollow oxygen at coverage 0.25 ML is 50 meV (400 cm^{-1}), as mentioned above. The deviation of *all* of our calculated frequencies to the experimental values indicates that the species giving rise to the high values measured experimentally is not any of the species we have considered here; i.e., it is not a single oxygen species located on the surface, in the surface-substitutional site, or in a subsurface site.

It is therefore hard to understand the proposed *atomic* nature and bond modes of the above-mentioned experimental results. Given that in the above two experiments, either a single-crystal surface or a polycrystalline material, have been exposed to oxygen under *high temperature* and *atmospheric pressure*, the substrates therefore will undergo a significant reconstruction. For further comparison with experiment, subsurface plus on-surface oxygen or even an oxidelike layer could be considered. Actually, our studies, which will be reported in detail elsewhere,[37] show that depending on the adsorption site, subsurface oxygen can stabilize on-surface oxygen and vice versa. And the strengthening of this interaction does result in a higher vibrational frequency [56 meV (455 cm^{-1}) and 65 meV (526 cm^{-1}) for on-surface and

subsurface oxygen, respectively[37]], but it is not nearly as high as these experimental values; also the vibrational frequency of O in Ag_2O (of 66 meV or 530 cm^{-1}) is also considerably lower than these reported experimental ones.[77]

VII. EFFECT OF STRAIN

In addition to various defects at the surface of "real catalysts," such as vacancies or steps, which affect the reactivity, there will likely be regions of strained material. Such regions could be induced by the defects, or by adsorption of thin films or adsorbates, thermal effects, or by atoms accumulated inside the substrate as recently identified occurs for argon in Ru(0001).[78] In this respect, experimental[78] and theoretical[79] work has highlighted the effect that strain can have on reactivity, in terms of the adsorption strength of adparticles. In particular, on tensile (expanded) substrates the adparticles were found to bond more strongly and, on compressive (contracted) substrates, to bond more weakly compared to the zero-strain situation.

From our results presented above, we have found that on-surface and surface-substitutional adsorption exhibit a different dependence of the adsorption energy on coverage, which indicates different lateral interactions between adsorbates, i.e., repulsive for on-surface adsorption for the whole coverage range considered, while for surface-substitutional adsorption, repulsive for coverages 0.11–0.25 ML and attractive for coverages 0.25–0.33 ML. In what follows we investigate the effect of strain for O in several sites, namely, (2×2) O/Ag(111) with O in the fcc-hollow site and $\sqrt{3}$ O/Ag(111) with O in the (symmetrical) surface-substitutional site. In these systems the lateral O interactions are repulsive and attractive, respectively. We further study the dependence on strain of O in the subsurface octahedral site with coverage 0.33 ML. In this structure the subsurface O-O interactions are at the transition point, changing from repulsive to attractive, for increasing coverages.[37] Tensile and compressive lateral strains of $\pm3\%$ are applied to the adsorbate-substrate systems, as well as to the clean relaxed surface in order to extract the adsorption energy. The top three metal layers and O are relaxed for all geometries.

The results are shown in Fig. 14 and in Table III. It can be seen that the effect of these small strains on the adsorption energies is quite significant. In particular, subsurface adsorption exhibits an increase of 0.30 eV for tensile strain. For on-surface and subsurface oxygen, the adsorption energy increases when a tensile strain is applied, which indicates that the interaction between O and Ag is strengthened; namely, it is energetically favorable to occupy the fcc-hollow site and subsurface octahedral site on the Ag substrate in the (expanded) tensile state. For surface-substitutional adsorption an *opposite* dependence has been found. The adsorption energy *decreases* with increasing distance between O atoms on the (expanded) tensile substrate. Conversely, for compressive strain, the adsorption energy of O in the fcc and subsurface sites decreases and that of surface-substitutional O increases. These trends for fcc and surface-substitutional sites are in line with the above-mentioned lateral interactions; i.e., under tensile strain the O atoms are farther apart which results in an
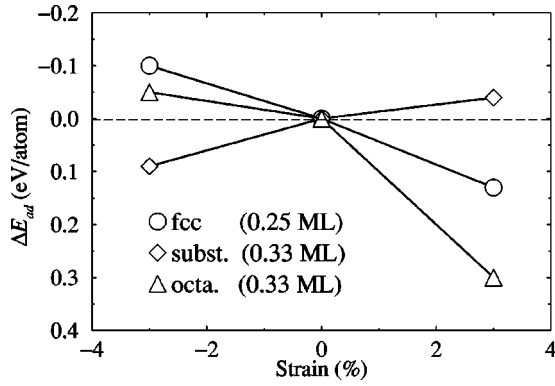
FIG. 14. Change of the adsorption energy with lateral strain for (2×2) O/Ag(111) with O in the fcc-hollow site (circles) and ($\sqrt{3} \times \sqrt{3})R30°$ O/Ag(111) for the surface-substitutional site (diamonds) and subsurface octahedral (triangles). A positive value of the strain corresponds to tensile and a negative value to compressive. The energy zero is the adsorption energy at zero strain and the reference system is the correspondingly strained, clean relaxed Ag(111) surface.

increase in binding energy for on-surface oxygen but a decrease for O in the surface-substitutional sites (see Figs. 1 and 8). For oxygen in the subsurface site, the adsorption energy is reduced for compressive strain. This is opposite to what is expected on the basis of the lateral interactions, which as noted above is attractive for higher coverage (closer distance between adatoms), indicating that an increase in adsorption energy would be expected. To understand the observed stain dependence, additional effects need to be considered: Experimentally, it has been found that oxygen prefers to adsorb on Ru(0001) with a tensile strain,[78] and theoretical investigations have proposed that the upshift of the d-band center, ϵ_d, with tensile strain is responsible for strengthening the interaction, and conversely that a downshift weakens the binding.[79] This concept has been generalized to other systems and as well as to facets and stepped surfaces by separating the effect into an electronic and a geometrical part.[73] We will apply this model to explain our results as follows.

For on-surface adsorption, the variation in bond length between oxygen and the first and second nearest-neighbor silver atoms, R_1 and R_2, is modest when either strain is applied, as shown in Table III. The change in the adsorption energy is therefore mainly from the electronic effect, where ϵ_d shifts down (up) with compressive (tensile) lateral strain. The tensile strain and upshift of ϵ_d empties more antibonding states and makes the interaction between oxygen and silver stronger. A shift of ϵ_d to lower energy leads to more antibonding states being occupied and weakens the interaction.

For surface-substitutional adsorption, the dependence of the position of ϵ_d on strain for the nearest-neighbor Ag atoms is similar to the on-surface adsorption, as shown in Table III. Unlike for on-surface adsorption, however, the O-Ag distance R_1 does not remain constant but increases for each applied strain. The position of ϵ_d for the second nearest-neighbor (surface) Ag atoms is practically unchanged for either strain. The second-neighbor bond length R_2, however,

TABLE III. The effect of strain for the fcc-hollow site with coverage 0.25 ML and the surface-substitutional (Subst.) site and subsurface octahedral (Sub. octa.) site with coverage 0.33 ML. R_1 and R_2 are the bond lengths between oxygen and its first and second nearest neighbors, respectively, followed by the center of the d band, ϵ_d, of the corresponding Ag atom. The unit is Å and the number given in brackets after the R's is the coordination number. ΔE_{ad} is the change in the adsorption energy with respect to the zero-strain result, in eV. For the subsurface site, the numbers (1 or 2) in parentheses indicate the (first or second) Ag layer to which O bonds.

		Strain (%)		
		Compressive		Tensile
		-3.0	0.0	3.0
fcc	$R_1(3)$	2.17	2.17	2.18
	ϵ_d^1	-4.38	-4.10	-3.94
	$R_2(3)$	3.60	3.68	3.76
	ϵ_d^2	-4.58	-4.36	-4.25
	ΔE_{ad}	-0.10	0.00	0.13
Subst.	$R_1(3)$	2.47	2.30	2.37
	ϵ_d^1	-4.35	-4.21	-4.07
	$R_2(6)$	2.92	3.05	3.13
	ϵ_d^2	-3.72	-3.71	-3.70
	ΔE_{ad}	0.09	0.00	-0.04
Sub. octa.	$R_1(3)$	2.29 (2)	2.29 (1)	2.29 (1)
	ϵ_d^1	-4.35 (2)	-3.96 (1)	-3.86 (1)
	$R_2(3)$	2.34 (1)	2.31 (2)	2.35 (2)
	ϵ_d^2	-3.79 (1)	-4.35 (2)	-4.11 (2)
	ΔE_{ad}	-0.05	0.00	0.30

decreases appreciably for compressive strain and strengthens the bond. This makes oxygen substitution in the substrate under compressive strain energetically favorable and overcompensates the electronic effect from the nearest-neighbor Ag atoms in the second layer which acts in reverse. Thus geometrical effects play the dominant role for this site.

For subsurface octahedral oxygen adsorption, the situation is more involved. In this case, oxygen bonds with three silver atoms in the first and second metal layers, and the difference between R_1 and R_2 is modest. For both compressive and tensile strain, the O-Ag bond lengths remain very similar, indicating that a geometrical effect is not the deciding factor for the result. (We first point out that for the zero-strain and tensile-strain situation, R_1 corresponds to Ag atoms in the first layer and R_2 to Ag atoms in the second layer. For compressive strain, however, the first and second neighboring Ag atoms are switched and R_1 corresponds to Ag atoms in the second layer and R_2 to those in the first.) For tensile strain, compared to the zero-strain situation, ϵ_d shifts up for both Ag atoms (i.e., in the first and second layers) as may be expected, and the interaction between oxygen and the substrate is notably strengthened (by a large 0.3 eV). For compressive strain, the variation of ϵ_d of the silver atom at the second metal layer (corresponding to R_1) is downwards, as for the other cases and as may be expected, which will act

to reduce the binding. However, the variation of ϵ_d of the silver atoms in the first layer, corresponding to R_2, is *not* downwards, but notably upwards, despite the fact that the lateral distance between the silver atoms is decreased, which usually tends to lower the ϵ_d. The reason for the upshift is the result of a geometrical effect in the sense that due to significant atomic relaxations, in response to the applied compressive strain, the topmost silver atoms move significantly outwards, away from the second metal layer (the first Ag-Ag interlayer spacing is now 3.10 Å as compared to 2.68 Å for zero strain). Thus their effective Ag coordination to the second layer is significantly reduced, giving rise to the upshift of ϵ_d, which will act to increase the binding. These different relative shifts of ϵ_d of the first- and second-layer Ag atoms will therefore have an opposite affect on the adsorption energy, where apparently the contribution from R_1 is stronger and gives rise to a modest decrease in binding energy.

Finally, we note that for surface-substitutional adsorption with oxygen bonded at the edge of the vacancy, the interaction between oxygen and silver is like the case of surface oxygen adsorption. It is therefore expected that the response to the strain will be similar as well. Indeed, we find that the adsorption energy increases by 0.06 eV when a 3% lateral tensile strain is applied, in contrast to what is observed for the high-symmetry site. The variation of R_1 and R_2 is modest, 2.22 and 2.56 Å, compared to 2.22 and 2.61 Å at zero strain, while the corresponding ϵ_d changes from -3.94 and -4.22 eV to -3.81 and -4.06 eV, respectively.

From the above discussions, we see that strain can notably affect the adsorption energy and that the effect is different for different sites. The result depends not only on the relative position of the substrate d band, but on the local atomic geometry of the adsorbate, and in addition, on the interrelationship between atomic relaxation and strain. In particular, as found for the subsurface site, depending on the details of the atomic relaxation of the system in response to the strain, an *opposite d*-band shift to that expected only on the basis of knowledge of the applied strain can result.

VIII. CONCLUSION

In the present paper we have systematically investigated the adsorption of atomic oxygen on the (111) surface of silver through first-principles DFT-GGA calculations. We considered a wide range of coverages for adsorption in the hcp- and fcc-hollow sites as well as surface-substitutional sites. The fcc-hollow site is energetically most favorable for the whole coverage range considered. The adsorption energy is found to be weak compared to adsorption on other transition metal surfaces (e.g., Ru, Rh) as may be expected. The relatively weak binding is due to the formation of bonding and antibonding states where the antibonding states are largely occupied. There is significant electron transfer from the substrate to the O atoms which results in a large increase in the work function. This yields a strong electrostatic repulsion between adsorbates which causes the adsorption energy to decrease with increasing coverage. With respect to oxygen in the gas phase, adsorption on the surface becomes unstable for coverages $\Theta > 0.5$ ML. In particular, the strong repulsion even at these lower coverages results in O preferring to adsorb in subsurface sites for coverages greater than about 0.25 ML.

For surface-substitutional adsorption, the interaction between oxygen adatoms is repulsive for low coverages, 0.11–0.25, and switches to attractive at higher coverages, 0.25–0.33, indicating island formation with a $\sqrt{3}$ structure. Compared to symmetric adsorption at the vacancy center, with O bonding to the three metal atoms in the second layer, it is energetically preferable for O to bond with two nearest-neighbor silver atoms at the edge of the vacancy for the $\sqrt{3}$ periodicity. In this configuration the *binding* energy becomes larger than for on-surface adsorption at the same coverage of 0.33 ML. At high temperatures and pressures it is possible that Ag vacancies could be created due to thermal energy and this $\sqrt{3}$ surface-substitutional structure might then form on regions of the surface. In particular, we find that adsorbed on-surface oxygen can considerably facilitate the formation of surface Ag vacancies. Our STM simulations for the $\sqrt{3}$ surface-substitutional structure shows good qualitative agreement with STM experiments performed on surfaces that have been exposed to high temperatures and high O_2 pressures. The other sites investigated—namely, on-surface and subsurface octahedral O—at the same coverage, exhibit qualitatively different features to experiment.

We also investigated the effect of strain and find that the adsorption energy exhibits a marked dependence on it (e.g., up to 0.3 eV increase for subsurface oxygen for a tensile strain of 3%) which is different for different sites: For on-surface adsorption, it is preferable to adsorb on the substrate in the tensile state due to the upshift of ϵ_d, while for surface-substitutional adsorption, a geometrical effect as opposed to an electronic effect plays the dominate role, and an increased interaction between oxygen and its second nearest neighbor makes the oxygen prefer to adsorb on the substrate in the compressive state. For subsurface octahedral oxygen, there is an interplay between electronic and geometrical effects which results in oxygen preferring to be located in the substrate in the tensile state.

In our future publication, for which the present paper lays the foundation for, we study various possible subsurface oxygen and bulk-dissolved oxygen species, as well as the most stable oxide, Ag_2O, and various surface oxidelike structures. These results will provide more insights into the O/Ag system and the behavior of Ag as an oxidation catalyst.

APPENDIX

Oxygen molecule

The oxygen pseudopotential is tested with respect to the cutoff radii and, with respect to the convergence it yields, of the physical properties of the oxygen molecule (binding energy, frequency, and bond length) concerning the energy cut-
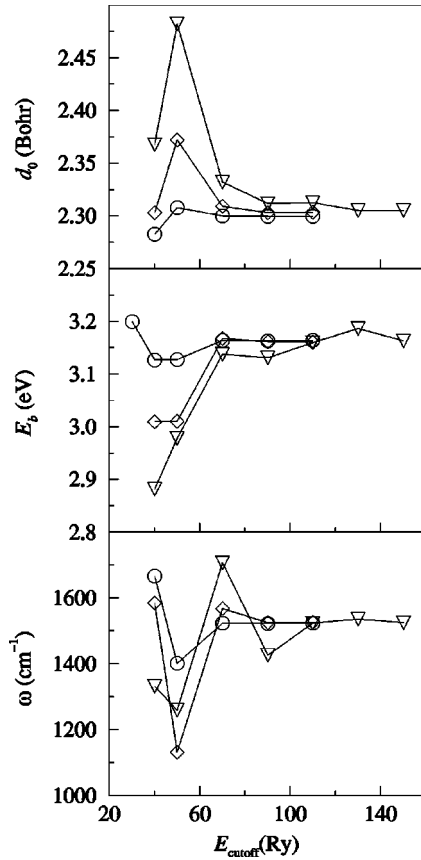
FIG. 15. The calculated bond length (top), binding energy per oxygen atom (middle), and frequency (bottom) of the oxygen molecule with respect to the energy cutoff for different pseudopotentials. The three different oxygen pseudopotentials have cutoff radii $r_s = r_p = r_d = 1.4$ (circles), 1.2 (diamonds), and 0.9 (triangles) bohr.

FIG. 16. The calculated binding energy with respect to atomic oxygen (upper) and bond length between O and Ag (lower) for (1 ×1) O/Ag(111) with 21 special **k** points in the IBZ as a function of energy cutoff for different pseudopotentials. Solid and open symbols represent the cutoff radii of the pseudopotentials, $r_s = r_p = r_d$ = 1.4 bohr and 1.2 bohr, while circles and diamonds indicate the results for the fcc- and hcp-hollow sites, respectively.

off, **k**-point sampling, and cell size. The Troullier-Martins scheme[41,42] is used to generate the pseudopotential within the GGA-PBE,[39] and three cutoff radii 0.9, 1.2, and 1.4 bohr are selected to represent typical hard, medium, and soft pseudopotentials. The total energy calculations are performed with a cubic box of side length 15 bohrs for both atomic and molecular oxygen, and the same result is obtained by further increase of the cube size to 20 bohrs. Three sets of **k** points—namely, the Γ point, the point (0.25, 0.25, 0.25), and six special **k** points in the IBZ—are used and the same results are obtained when the energy cutoff is larger than 50 Ry. The spin-polarization correction of atomic oxygen is −1.60 eV. For an un-spin-polarized calculation of molecular oxygen, the obtained ground state is a singlet, corresponding to the first excited state of O_2, which is 0.90 eV higher than the real ground state (triplet). Both of these two factors are taken into account in our calculations. The results obtained with the (0.25, 0.25, 0.25) point are presented and used to extract the binding energy of oxygen adsorption on the Ag(111) surface.

The calculated binding energy, bond length, and frequency of molecular oxygen are shown in Fig. 15. We can see that the oxygen pseudopotential with cutoff radius 1.4 bohr presents the best convergence, and the convergence is

essentially complete for 70 Ry. The hardest pseudopotential with cutoff radius 0.9 bohr approaches practically the same number when E_{cutoff} is sufficiently large. We obtain the following converged results: $1/2E_b^{O_2} = 3.16$ eV/atom, $d_0 = 2.30$ bohrs, and $\omega = 189$ meV (1523 cm^{-1}). The respective experimental results are 2.56 eV, 2.28 bohrs, and 197 meV (1586 cm^{-1}),[57] while the binding energy calculated by Perdew *et al.* with the same GGA-PBE is 3.12 eV.[39] The calculated bond length and frequency agree very well with the experimental results. Despite the overbinding of the calculated binding energy, the different theoretical methods give essentially the same result. These results clearly indicate that the overbinding is from the exchange-correlation approximation in DFT and is independent of the framework of the total energy calculations. The error is a systematic error. Furthermore, the overbinding is independent of the construction of the pseudopotential, and soft pseudopotentials can be safely used in the total energy calculations. Despite the overbinding, the other properties of the bond length and vibrational frequency can be well described by DFT.

Oxygen adsorption

Further tests concerning the effect of the oxygen pseudopotential, energy cutoff, and **k** points on adsorption of O have been performed. We used the (1×1) supercell with a five-layer slab separated by 15 Å of vacuum space to describe the Ag(111) surface. Twenty-one special **k** points in

the IBZ are used, and oxygen is put on one side of the slab, where the dipole moment correction is taken into account.[45] Structural relaxation for the top two metal layers is included for all geometries. Both the fcc- and hcp-hollow sites are considered, and the binding energies and bond lengths between oxygen and silver are presented in Fig. 16 for two different oxygen pseudopotentials: namely, with cutoff radii of 1.2 and 1.4 bohr. The soft pseudopotential, 1.4 bohr, presents a better convergence, as expected. The binding energy has already completely converged at 50 Ry, while for the bond length, with further increase to 70 Ry, it decreases by only 0.01 Å. For the hard pseudopotential, 1.2 bohr, the binding energy approaches the same value at 70 Ry, and the bond

length is essentially the same as that obtained with the soft pseudopotential. As clearly shown in Fig. 16, despite the fact that the absolute value of the binding energy is not completely converged at 50 Ry, the relative stability between fcc- and hcp-hollow sites converges well (less than 0.01 eV per adatom), and the change in bond length is not larger than 0.02 Å. When the special **k** points in the IBZ increase from 21 to 30, the change of the binding energy and bond length between oxygen and silver for the fcc-hollow site is 0.002 eV and 0.001 Å respectively, i.e., negligible. As a conclusion, we use the oxygen pseudopotential with cutoff radius 1.4 bohr and a 50 Ry energy cutoff in the present and future work.

[1] R. A. van Santen and H. P. C. E. Kuipers, Adv. Catal. **35**, 265 (1987).

[2] R. B. Grant and R. M. Lambert, Surf. Sci. **146**, 256 (1984); J. Catal. **92**, 364 (1985).

[3] C. B. Wang, G. Deo, and I. E. Wachs, J. Phys. Chem. B **103**, 5645 (1999).

[4] D. I. Kondarides, G. N. Papatheodorou, C. G. Vayenas, and X. E. Vergkios, Ber. Bunsenges. Phys. Chem. **97**, 709 (1993).

[5] V. I. Avdeev, A. I. Boronin, S. V. Koscheev, and G. M. Zhidomirov, J. Mol. Catal. A: Chem. **154**, 257 (2000), and references therein.

[6] V. I. Bukhtiyarov, M. Hävecker, V. V. Kaichev, A. Knop-Gericke, R. W. Mayer, and R. Schlögl (unpublished); V. I. Bukhtiyarov, M. Hävecker, V. V. Kaichev, A. Knop-Gericke, R. W. Mayer, and R. Schlögl, Catal. Lett. **74**, 121 (2001), and references therein.

[7] X. Bao, M. Muhler, Th. Schedel-Niedrig, and R. Schlögl, Phys. Rev. B **54**, 2249 (1996), and references therein.

[8] D. Herein, A. Nagy, H. Schubert, G. Weinberg, E. Kitzelmann, and R. Schlögl, Z. Phys. Chem. (Munich) **197**, S67 (1996).

[9] G. Rovida, F. Pratesi, M. Maglietta, and E. Ferroni, Surf. Sci. **43**, 230 (1974).

[10] C. T. Campbell, Surf. Sci. **157**, 43 (1985).

[11] C. T. Campbell, Surf. Sci. **173**, L641 (1986).

[12] F. Buatier de Mongeot, U. Valbusa, and M. Rocca, Surf. Sci. **339**, 291 (1995); M. Rocca, F. Cemič, F. Bautier de Mongeot, U. Valbusa, S. Lacombe, and K. Jacobi, ibid. **373**, 125 (1997).

[13] S. Bare, K. Griffiths, W. N. Lennard, and H. T. Tang, Surf. Sci. **342**, 185 (1995).

[14] C. I. Carlisle, D. A. King, M. L. Bocquet, J. Cerdá, and P. Sautet, Phys. Rev. Lett. **84**, 3899 (2000).

[15] C. I. Carlisle, T. Fujimoto, W. S. Sim, and D. A. King, Surf. Sci. **470**, 15 (2000).

[16] C. Rehren, M. Muhler, X. Bao, R. Schlögl, and G. Ertl, Z. Phys. Chem. (Munich) **174**, 11 (1991).

[17] X. Bao, M. Muhler, B. Pettinger, R. Schlögl, and G. Ertl, Catal. Lett. **22**, 215 (1993).

[18] B. Pettinger, X. Bao, I. C. Wilcock, M. Muhler, and G. Ertl, Phys. Rev. Lett. **72**, 1561 (1994).

[19] X. Bao, J. V. Barth, G. Lehmpfuhl, R. Schuster, Y. Uchida, R. Schlögl, and G. Ertl, Surf. Sci. **284**, 14 (1993).

[20] H. Schubert, U. Tegtmeyer, D. Herein, X. Bao, M. Muhler, and R. Schlögl, Catal. Lett. **33**, 305 (1995).

[21] Th. Schedel-Niedrig, X. Bao, M. Muhler, and R. Schlögl, Ber. Bunsenges. Phys. Chem. **101**, 994 (1997).

[22] H. Schubert, U. Tegtmeyer, and R. Schlögl, Catal. Lett. **28**, 383 (1994).

[23] D. Zemlyanov and R. Schlögl, Surf. Sci. **470**, L20 (2000); D. Zemlyanov, A. Nagy, and R. Schlögl, Appl. Surf. Sci. **133**, 171 (1998).

[24] M. Scheffler and C. Stampfl, in *Electronic Structure*, Vol. 2 of *Handbook of Surface Science*, edited by K. Horn and M. Scheffler (Elsevier, Amsterdam, 1999).

[25] P. J. van den Hoek, E. J. Baerends, and R. A. van Santen, J. Phys. Chem. **93**, 6469 (1989).

[26] E. A. Carter and W. A. Goddard III, Surf. Sci. **209**, 243 (1989).

[27] H. Nakatsuji, Prog. Surf. Sci. **54**, 1 (1997).

[28] V. I. Avdeev, S. F. Ruzankin, and G. M. Zhidomirov, J. Struct. Chem. **38**, 519 (1997); V. I. Avdeev and G. M. Zhidomirov, *ibid.* **40**, 343 (1999).

[29] C. Saravanan, M. R. Salazar, J. D. Kress, and A. Redondo, J. Phys. Chem. B **104**, 8685 (2000).

[30] J. Torras, M. Toscano, J. M. Ricart, and N. Russo, J. Mol. Catal. **119**, 387 (1997).

[31] M. A. Milov, I. L. Zilberberg, S. Ph. Ruzankin, and G. M. Zhidomirov, J. Mol. Catal. **158**, 309 (2000).

[32] D. Sekiba, H. Nakamizo, R. Ozawa, Y. Gunji, and H. Fukutani, Surf. Sci. **449**, 111 (2000).

[33] V. I. Pazzi, P. H. T. Philipsen, E. J. Baerends, and G. F. Tantardini, Surf. Sci. **443**, 1 (1999).

[34] M. R. Salazar, C. Saravanan, J. D. Kress, and A. Redondo, Surf. Sci. **449**, 75 (2000); M. R. Saravanan, J. D. Kress, and A. Redondo, Catal. Lett. **64**, 107 (2000).

[35] M. R. Salazar, J. D. Kress, and A. Redondo, Surf. Sci. **469**, 80 (2000).

[36] P. A. Gravil, D. M. Bird, and J. A. White, Phys. Rev. Lett. **77**, 3933 (1996); D. M. Bird and P. A. Gravil, Surf. Sci. **377-379**, 555 (1997).

[37] W. X. Li, C. Stampfl, and M. Scheffler (unpublished).

[38] M. Bockstedte, A. Kley, J. Neugebauer, and M. Scheffler, Comput. Phys. Commun. **107**, 187 (1997).

[39] J. P. Perdew, K. Burke, and M. Ernzerhof, Phys. Rev. Lett. **77**, 3865 (1996).

[40] J. A. White and D. M. Bird, Phys. Rev. B **50**, 4954 (1994).

[41] M. Fuchs and M. Scheffler, Comput. Phys. Commun. **116**, 1 (1999).

[42] N. Troullier and J. L. Martins, Phys. Rev. B **43**, 1993 (1991).

[43] M. Fuchs, M. Bockstedte, E. Pehlke, and M. Scheffler, Phys. Rev. B **57**, 2134 (1998).

[44] X. Gonze, R. Stumpf, and M. Scheffler, Phys. Rev. B **44**, 8503 (1991); X. Gonze, P. Käckell, and M. Scheffler, *ibid.* **41**, 12 264 (1990).

[45] J. Neugebauer and M. Scheffler, Phys. Rev. B **46**, 16 067 (1992).

[46] S. L. Cunningham, Phys. Rev. B **10**, 4988 (1974).

[47] In obtaining the DOS we do not apply a cutoff radius for the pseudo wave functions. We varified that qualitatively the same results are obtained when applying a cutoff of 2.2 bohrs, indicating that the DOS are largely independent of the arbitrary cutoff radius.

[48] V. L. Moruzzi, J. F. Janak, and K. Schwarz, Phys. Rev. B **37**, 790 (1988).

[49] A. Khein, D. J. Singh, and C. J. Umrigar, Phys. Rev. B **51**, 4105 (1995).

[50] B. D. Yu and M. Scheffler, Phys. Rev. B **55**, 13 916 (1997).

[51] H. M. Polatoglou, M. Methfessel, and M. Scheffler, Phys. Rev. B **48**, 1877 (1993).

[52] C. Kittel, *Introduction to Solids State Physics*, 7th ed. (Wiley, New York, 1996).

[53] E. A. Soares, V. B. Nascimento, V. E. de Carvalho, C. M. C. de Castilho, A. V. de Carvalho, R. Toomes, and D. P. Woodruff, Surf. Sci. **419**, 89 (1999).

[54] E. A. Soares, G. S. Leatherman, R. D. Diehl, and M. A. Van Hove, Surf. Sci. **468**, 129 (2000).

[55] M. Chelvayohan and C. H. B. Mee, J. Phys. C **15**, 2305 (1982).

[56] M. Fuchs and C. Müller (private communication).

[57] K. P. Huber and G. Herzberg, *Molecular Spectra and Molecular Structure IV: Constants of Diatomic Molecules* (Van Nostrand Reinhold, New York, 1979).

[58] C. Stampfl and M. Scheffler, Phys. Rev. B **54**, 2868 (1996).

[59] M. V. Ganduglia-Pirovano and M. Scheffler, Phys. Rev. B **59**, 15 533 (1999).

[60] C. Stampfl, H. J. Kreuzer, S. H. Payne, H. Pfnür, and M. Scheffler, Phys. Rev. Lett. **83**, 2993 (1999).

[61] C. Stampfl, S. Schwegmann, H. Over, M. Scheffler, and G. Ertl, Phys. Rev. Lett. **77**, 3371 (1996).

[62] K. D. Gibson, M. Viste, E. C. Sanchez, and S. J. Sibener, J. Chem. Phys. **110**, 2757 (1999).

[63] C. Stampfl and M. Scheffler (unpublished).

[64] A. L. Allred, J. Inorg. Nucl. Chem. **17**, 215 (1961); L. Pauling, *The Nature of the Chemical Bond*, 3rd ed. (Cornell University, Ithaca, NY, 1960).

[65] T. Zambelli, J. Wintterlin, J. Trost, and G. Ertl, Science **273**, 1688 (1996).

[66] B. Hammer, Phys. Rev. Lett. **83**, 3681 (1999).

[67] D. M. Ceperley and B. J. Alder, Phys. Rev. Lett. **45**, 566 (1980); J. P. Perdew and A. Zunger, Phys. Rev. B **23**, 5048 (1981).

[68] E. A. Soares, C. Bittencourt, V. B. Nascimento, V. E. de Carvalho, C. M. C. de Castilho, C. F. McConville, A. V. de Carvalho, and D. P. Woodruff, Phys. Rev. B **61**, 13 983 (2000).

[69] S. Oppo, V. Fiorentini, and M. Scheffler, Phys. Rev. Lett. **71**, 2437 (1993).

[70] S. A. de Vries, W. J. Huisman, P. Goedtkindt, M. J. Zwanenburg, S. L. Bennett, I. K. Robinson, and E. Vlieg, Surf. Sci. **414**, 159 (1998).

[71] P. Bailey, T. C. Q. Noakes, and D. P. Woodruff, Surf. Sci. **426**, 358 (1999).

[72] A. Nagy, G. Mestl, D. Herein, G. Weinberg, E. Kitzelmann, and R. Schlögl, J. Catal. **182**, 417 (1999).

[73] B. Hammer and J. K. Nørskov, Adv. Catal. **45**, 71 (2000).

[74] A. Eichler and J. Hafner, Phys. Rev. B **62**, 5163 (2000).

[75] J. Tersoff and D. R. Hamann, Phys. Rev. B **31**, 805 (1985).

[76] N. D. Lang, Comments Condens. Matter Phys. **14**, 253 (1989).

[77] B. Pettinger, X. Bao, I. Wilcock, M. Muhler, B. Pettinger, R. Schlögl, and G. Ertl, Angew. Chem. Int. Ed. Engl. **33**, 85 (1994).

[78] M. Gsell, P. Jacob, and D. Menzel, Science **280**, 717 (1998).

[79] M. Mavrikakis, B. Hammer, and J. K. Nørskov, Phys. Rev. Lett. **81**, 2819 (1998).